Comprehensive assessment of meteorological conditions and airflow connectivity during HCCT-2010

A. Tilgner[1], L. Schöne[1], P. Bräuer[1], D. van Pinxteren[1], E. Hoffmann[1], G. Spindler[1], S. A. Styler[1], S. Mertes[1], W. Birmili[1], R. Otto[1], M. Merkel[1], K. Weinhold[1], A. Wiedensohler[1], H. Deneke[1], R. Schrödner[1], R. Wolke[1], J. Schneider[2], W. Haunold[3], A. Engel[3], A. Wéber[3], and H. Herrmann[1]

[1]{Leibniz Institute for Tropospheric Research (TROPOS), Leipzig, Germany}

[2]{Particle Chemistry Department, Max Planck Institute for Chemistry, Mainz, Germany}

[3]{Institute for Atmospheric and Environmental Sciences (IAU), Goethe University Frankfurt, Germany}

Correspondence to: H. Herrmann (herrmann@tropos.de)

Abstract

This study presents a comprehensive assessment of the meteorological conditions and atmospheric flow during the Lagrangian-type "Hill Cap Cloud Thuringia 2010" experiment (HCCT-2010), which was performed in September and October 2010 at Mt. Schmücke in the Thuringian Forest, Germany and which used observations at three measurement sites (upwind, in-cloud, and downwind) to study physical and chemical aerosol–cloud interactions. A Lagrangian-type hill cap cloud experiment requires not only suitable cloud conditions but also connected airflow conditions (*i.e*. representative air masses at the different measurement sites). The primary goal of the present study was to identify time periods during the 6-week duration of the experiment in which these conditions were fulfilled and therefore which are suitable for use in further data examinations. The following topics were studied in detail: i) the general synoptic weather situations, including the mesoscale flow conditions ii) local meteorological conditions and iii) local flow conditions. The latter were investigated by means of statistical analyses using best-available quasi-inert tracers, SF_6 tracer experiments in the experiment area, and regional modelling. This study represents the first application of comprehensive analyses using statistical measures such as the coefficient of divergence

(COD) and the cross-correlation in the context of a Lagrangian-type hill cap cloud experiment. This comprehensive examination of local flow connectivity yielded a total of 14 full-cloud events (FCEs), which are defined as periods during which all connected flow and cloud criteria for a suitable Lagrangian-type experiment were fulfilled, and 15 non-cloud events (NCEs), which are defined as periods with connected flow but no cloud at the summit site, and which can be used as reference cases. The overall evaluation of the identified FCEs provides the basis for subsequent investigations of the measured chemical and physical data during HCCT-2010 (see http://www.atmos-chem-phys.net/special_issue287.html).

Results obtained from the statistical flow analyses and regional-scale modelling performed in this study indicate the existence of a strong link between the three measurement sites during the FCE and NCE events, particularly under conditions of constant south-westerly flow, high wind speeds and slightly stable stratification. COD analyses performed using continuous measurements of ozone and particle (49 nm diameter size bin) concentrations at the three sites revealed, particularly for COD values < 0.1, very consistent time series (*i.e.* close links between air masses at the different sites). The regional scale model simulations provided support for the findings of the other flow condition analyses. Cross-correlation analyses revealed typical overflow times of ~15–30 min between the upwind and downwind valley sites under connected flow conditions. The results described here, together with those obtained from the SF_6 tracer experiments performed during the experiment, clearly demonstrate that a) under appropriate meteorological conditions a Lagrangian-type approach is valid and b) the connected flow validation procedure developed in this work is suitable for identifying such conditions. Overall, it is anticipated that the methods and tools developed and applied in the present study will prove useful in the identification of suitable meteorological and connected airflow conditions during future Lagrangian-type hill cap cloud experiments.

1 Introduction

Clouds occupy on average ~15% of the volume of the lower troposphere (Pruppacher and Jaenicke, 1995) and play a crucial role in the various physical and chemical processes occurring there (Heintzenberg and Charlson, 2009; Möller, 2010; Ravishankara 1997). Thus, physical and chemical cloud processes influence large-scale environmental issues such as climate change and, by extension, have a variety of societal implications (Boucher et

al., 2013). Since both the spatial and temporal occurrence and the altitude of clouds are highly variable, investigations of physical and chemical interactions between gases, aerosol particles and cloud droplets are quite challenging. Consequently, these interactions are much less understood than pure gas-phase processes. Several hill cap cloud experiments conducted in the past (at Kleiner Feldberg, Germany, in 1990 (Wobrock et al., 1994); at Great Dun Fell, United Kingdom, in 1993 and 1995 (Bower et al., 1999; Choularton et al., 1997); at Tenerife, Spain, in 1997 (Bower et al., 2000); and at Mt. Schmücke, Germany, in 2001 and 2002 (Herrmann et al., 2005)) have shown that ground-based Lagrangian-type experiments, where an orographic cloud is used as a natural flow-through reactor, provide a valuable opportunity to study cloud processes in detail.

Ground-based cloud experiments offer the opportunity to characterise the gas phase, the aerosol particle phase, and the cloud droplet phase in much experimental detail before, during and after cloud processing, and thus enable an advanced understanding of chemical cloud effects and interactions. However, the use and quality of Lagrangian-type hill cap cloud field campaigns strongly depends on meteorological conditions: without a connected flow, comparisons of the physical and chemical properties of aerosol upwind and downwind of a cloud are meaningless. For this reason, successful investigation of datasets obtained during these experiments requires as a necessary condition a critical evaluation of meteorological and flow connectivity conditions (see Tilgner et al., 2005; Heinold et al., 2005).

In the present study, so-called “connected flow conditions” are defined as conditions where the incoming flow passes the upwind area and subsequently the mountain ridge before finally reaching the downwind area. It is explicitly noted here that “connected flow conditions” do not necessarily require an air parcel trajectory to connect all three sampling sites, as these sites were designed to measure representative aerosol compositions in the upwind, summit and downwind areas. In general, hill cap cloud experiments make use of the fact that air parcels can be forced to traverse a hill or a mountain ridge and that—under favourable conditions—the terrain-induced lifting cools down the air parcel so that an orographic cloud is formed near the mountain ridge. Under these “natural flow-through reactor” conditions, the cloud-induced changes to the concentrations of both particle- and gas-phase compounds can be characterised by ground-based field measurements conducted upwind, in-cloud, and downwind of the mountain ridge.

The connectivity of atmospheric flow across a mid-level mountain ridge can be evaluated using non-dimensional parameters like the Froude and Richardson numbers (see Heinold et al., 2005 and references therein). These parameters can be derived from measurements of the horizontal wind field and the vertical stratification. An essential question is whether the incoming air parcel contains enough kinetic energy (*i.e.* wind speed) to ascend and pass over the mountain ridge under a given set of vertical thermal conditions. Thus, vertical stratification and wind shear come into play as well. In reality, the evaluation of flow connectivity can be complicated by wind shear and by non-homogeneous terrain, such as a variable crest line and changing surface roughness. For these reasons, other local parameters also need to be used to assess the likelihood of an air parcel passing over a mountain ridge.

The movement of an air parcel across a mountain ridge can also be ascertained using continuously measured tracer species. These tracer species can include, for example, relatively inert gas-phase species, such as ozone (O_3), and atmospheric aerosol particles that are not expected to be modified by a cloud passage, such as interstitial particles of a certain size. Another method for validation of flow connectivity is provided by dedicated introduced inert tracer experiments, which are typically performed only occasionally during measurement campaigns (see Heinold et al., 2005 and references therein).

In order for equivalent, and thus comparable, air masses to exist at all sites, measurement periods must not be affected by air mass changes (*i.e.* front passages) or precipitation. For this reason, an assessment of the synoptic and local meteorological conditions must also be included in an evaluation of the overall suitability of a given set of conditions for further investigation of cloud passage experiment data.

The present work intends to perform a comprehensive assessment of meteorological conditions and flow connectivity during the Hill Cap Cloud Thuringia (HCCT-2010) experiment in order to provide evaluated periods with both adequate meteorological conditions and flow connectivity. Since fulfilment of these conditions is a prerequisite for meaningful comparisons of the physical and chemical aerosol properties measured in the upwind (before the cloud interaction), summit (inside the cloud), and downwind (after the cloud interaction) regions, the comprehensive analysis presented here is of major importance both for previously published works and for additional further studies performed using data obtained during HCCT-2010 *(e.g.* those contained in the HCCT-2010 Special Issue, http://www.atmos-chem-phys.net/special_issue287.html). Moreover, the methodology used

and applied here is of a wider scientific interest for the design and interpretation of Lagrange-type hill-cap cloud experiments.

HCCT-2010 was conducted in September and October 2010 at Mt. Schmücke (937 m amsl), which is part of the mountain ridge of the Thuringian Forest (Germany). This location was previously used for the hill cap cloud campaign FEBUKO (Field Investigations of Budgets and Conversions of Particle Phase Organics in Tropospheric Cloud Processes; see Herrmann et al., 2005 for further details), in which the local meteorological conditions and airflow characteristics were studied extensively (Tilgner et al., 2005; Heinold et al., 2005). During FEBUKO, model calculations and tracer experiments showed that the flow between the measurement sites was reasonably well-connected during many cloud events.

In preparation for HCCT-2010, we re-evaluated results obtained during the FEBUKO study and also examined more recent meteorological data (2004–2008). In these evaluations, we found that the maximum probability for hill cap clouds to occur in the area occurred during September and October. This run-up analysis showed, for example, that on 5-year-average, approximately 10 cloud events occurred per month in each of September and October under suitable wind conditions (*i.e.* southwesterly (SW) wind direction). From this analysis, it was decided to conduct HCCT-2010 during September and October 2010, as these months provided the highest probability of occurrence of warm orographic clouds in connection with SW flow (*i.e.* flow traversing the mountain range in perpendicular fashion).

In analogy to the previous studies performed at Mt. Schmücke (see Tilgner et al., 2005; Heinold et al., 2005), the present work examines the synoptic conditions, flow connectivity and other meteorological issues important for the experimental concept of the hill cap cloud experiment HCCT-2010. First, the mesoscale conditions were evaluated, with particular attention paid to the incident flow conditions and the properties of the air masses advected into the HCCT-2010 study area. Then, the properties of the local airflow were analysed in detail. In particular, the connectivity of atmospheric flow across the mountain ridge was assessed using meteorological, aerosol, and gas-phase parameters measured upwind, on top, and downwind of the mountain ridge. The entire measurement period was analysed using statistical measures with respect to the prevalence of the same air mass at all sites, irrespective of wind direction and the presence or absence of an orographic cloud. Classification criteria were then developed concerning two main issues: (i) whether the airflow was likely to be connected between the three observation areas across the mountain ridge and (ii) whether a

hill cap cloud was present and therefore likely to have influenced the air parcel travelling across the ridge. All selected reference periods (i.e., FCEs see below) of HCCT-2010 are further evaluated with respect to the question of flow connectivity and cloud conditions. Both calculations of non-dimensional flow parameters (*e.g.* the Froude number (Fr)) and simulations performed using the COSMO meteorological forecast model (COnsortium for Small-scale MOdelling (Baldauf et al., 2011; Schättler et al., 2012)) were used to characterise the regional flow regime in the mountainous terrain. For several specific periods, the airflow was verified using dedicated tracer experiments, which were performed using the inert gas SF_6. In addition, locally measured meteorological and microphysical data, rawinsonde observations, satellite pictures, ceilometer data and calculated backward trajectories were used to identify orographic/non-orographic cloudiness, to detect frontal processes, and to characterise both the air mass advection and the cloud conditions during the selected event periods. Finally, these meteorological and connected flow investigation results were used to comprehensively identify periods, here referred to as full-cloud events (FCEs) and non-cloud events (NCEs), suitable for use in further investigations. Here, FCEs are defined as periods where all predefined connected flow and cloud criteria for a suitable Lagrangian-type experiment were fulfilled (see Section 3.2 for details), while NCEs are defined as periods with connected flow conditions but without clouds present at any of the three measurement sites.

2 Methods and implementation

2.1 Measurement site description

HCCT-2010 was conducted at Mt. Schmücke in Thuringia, Germany, during September and October 2010. The summit of Mt. Schmücke belongs to the mid-height mountain ridge of the Thuringian Forest, which runs northwest to southeast for ~60 km without any major gaps. Based on results obtained during the FEBUKO experiment (see Heinold et al., 2005), three ground-based measurement sites were established during HCCT-2010: Goldlauter (GL, nominal upwind site), Mt. Schmücke (SM, summit site), and Gehlberg (GB, nominal downwind site) (see Fig. 1). The upwind site Goldlauter (10° 45’ 20’’ E, 50° 38’ 25’’ N, 605 m amsl) served as the location for characterisation of air parcels approaching the experimental site under south-western (SW) flow conditions. The summit site Mt. Schmücke (10° 46’ 15’’ E, 50° 39’ 19’’ N, 937 m amsl), where the German Weather Service (Deutscher

Wetterdienst, DWD) and the Federal Environmental Office (Umweltbundesamt, UBA) operate a research station, served as the primary location for analysis of physical and chemical aerosol and cloud droplet parameters. The site is located near the mountain ridge, and Mt. Schmücke itself is in the vicinity of the highest peak of the Thuringian Forest (982 m amsl). Finally, the downwind site Gehlberg (10° 47' 32'' E, 50° 40' 21'' N, 732 m amsl) served as the location for characterisation of air masses descending the downwind slope of the Thuringian Forest mountain ridge under appropriate SW flow conditions.

The topography in the measurement area is quite complex (see Figure 1). The terrain is characterised by a rather narrow valley, wherein the upwind site Goldlauter is located, and two downwind valleys, which begin uphill of the downwind site Gehlberg. Since they permit diverging flow, these valleys can complicate the connected flow conditions. However, previous tracer experiments (Heinold et al., 2005) have shown that, under suitable flow conditions, representative air masses from the upwind area are able to reach the downwind site.

Offline sampling (*i.e.* experimental measurements with all instruments not running continuously) was performed only under specific suitable conditions. Based on the results obtained during the FEBUKO experiment (Herrmann et al., 2005), the following six criteria were used to determine appropriate time periods for offline sampling during HCCT-2010 in the context of a Lagrangian-type hill cap cloud experiment: (i) liquid water content (LWC) of the summit site cloud above 0.1 g m^{-3} (ii) wind direction from the south-west (200°–250° sector) (iii) wind speed at Mt. Schmücke of at least 2 m s^{-1} and not exceeding 12 m s^{-1} (iv) no fog at the two valley sites (v) no precipitation at any site and (vi) air temperature above 0°C. Further details on these required condition criteria are outlined in Herrmann et al. (2005).

2.2 Characterisation of the local flow connectivity using coefficient of divergence (COD) of particles in the Aitken (49 nm) and accumulation mode (217 nm) range

During HCCT-2010, particle number size distributions were recorded continuously at all three sites using four identical scanning mobility particle sizers (SMPS). Selected particle size bins were used in the present study for characterisation of the local flow connectivity. Details regarding the SMPS measurements are given in the electronic supplementary material (ESM).

In order to investigate spatial variation in selected aerosol size bins between two measurement sites and thus to characterise the degree of similarity between particle data, the coefficient of divergence (COD, sometimes also abbreviated as CD) was used as a statistical measure. This measure has been used in several studies (see e.g., Wongphatarakul et al., 1998; Pinto et al. 2004; Krudysz et al. 2008; Ott et al. 2008; Wang et al. 2011) to determine the relative spatial variability of measured particle mass and constituent concentrations between different sampling sites. In the present study, the COD was used to characterise the temporal similarities between measured particle data at the different HCCT-2010 sites and thus to provide information regarding the airflow over the mountain range. The COD is defined as

$$COD_{a,b} = \sqrt{\frac{1}{n}\sum_{i=1}^{n}\left(\frac{x_{i,a}-x_{i,b}}{x_{i,a}+x_{i,b}}\right)^2} \quad (1)$$

where x_{ia} and x_{ib} represent the *i*-th aerosol number concentrations measured at sites a and b, respectively, and n represents the total number of data points considered in the calculation. In cases where the obtained concentrations at the two sampling sites are very similar, the COD approaches zero. By contrast, in cases where the concentration profiles at two sites differ, the COD approaches unity. It should be noted that the COD represents a measure for comparison of two sites only and therefore cannot be used in the present study to compare all three measurement sites at once. Therefore, for an overall comparison of the three HCCT-2010 sites, the COD of each site combination was calculated; then, all three COD values were compared to a threshold value that indicates similarity between particle data and, by extension, connected flow conditions between the three measurement sites.

The US Environmental Protection Agency (US EPA, 2004) has proposed a COD criterion for the characterisation of the uniformity between aerosol data sets. According to this criterion, COD values larger than 0.2 indicate dataset heterogeneity, while COD values below 0.1 indicate dataset homogeneity. This criterion is in agreement with other studies reported in the literature, which have used a COD of 0.2 as a reference value (see the above-mentioned COD references). In the context of overflow characterisation, this means that lower CODs indicate good flow connectivity conditions, while larger CODs indicate conditions without connected flow (and thus conditions unsuitable for further investigations).

In the present study, a floating 3-hour time span of the measured aerosol number concentrations (*i.e.* an interval of 3 hours centred around the time point of interest) was used

for the calculation of the COD at a given time. Two specific particle diameter bins of the SMPS number size distribution were used for the characterisation of flow connectivity: 49 nm and 217 nm. The particle number concentration in the 49 nm diameter bin (N_{49nm}) was selected because this bin represents the upper size range of the aerosol particles that tend to be unaffected by cloud activation. In addition, these particles tend to be substantially less affected by coagulation and diffusion processes than smaller particles. In the case of connected flow, therefore, one would expect low COD values for this parameter. The particle number density in the 217 nm diameter bin (N_{217nm}) was used to assess the likelihood of in-cloud particle activation, since particles of this size are very likely to be activated in the presence of a cloud, and thus disappear from the interstitial aerosol. Thus, larger COD values for this size bin were used in concert with LWC measurements at the summit site as indicators of fog conditions at the three sites. It should be noted here that the measured N_{217nm} values could be slightly affected during the overflow by processes including dry/wet deposition, collision/coagulation, chemical in-cloud mass production and entrainment processes.

The calculated CODs for the different pairs of the three measurement sites and the two aerosol particle size bins are presented in Section 3 and given in table form in the ESM. No time lag between the time series associated with the three measurement sites was applied in these COD calculations. The overall goal of the COD analysis was to identify potentially suitable time periods in an objective and automatic manner. The consideration of predefined assumptions such as a fixed time lag between the different sites contradicts this idea and thus – a priori - it was not possible to include such a time lag. In addition, the magnitude of the time lag varies temporally and, depending on the incoming flow conditions (southwest and northeast wind direction), may be positive or negative. Moreover, the magnitude of the time lags between the sites is typically small compared to the 3-hour time span applied for the COD calculation (see Section 3.2.1). Thus, an applied short-term time lag between the time series (according to the transport time between the sites) do not have a huge impact on the obtained results.

2.3 Characterisation of the local flow connectivity using measured ozone concentrations

Local measurements of trace gas concentrations can be used to complement particle-based characterisations of the local flow connectivity. A suitable tracer for this purpose must be quasi-inert (*i.e.* unaffected by chemical decay and deposition during transport on the spatial scale of the experiment) and, in addition, highly variable in both time and space. In previous hill cap cloud campaigns, including the Great Dun Fell experiment (Colvile et al., 1997) and the FEBUKO experiment (Herrmann et al., 2005), ozone was shown to be an appropriate quasi-inert tracer. The reason for this is twofold: first, ozone is only secondarily produced in the troposphere and has no primary direct emission sources; second, since ozone is characterised by low water solubility (Henry's Law constant of only $\sim 1.0 \cdot 10^{-2}$ M atm^{-1}, see Sander, 1999 and references therein), it is consumed only ineffectively in acidic continental clouds. Overall, these properties recommend ozone as a suitable quasi-inert tracer for the present connected flow analysis.

During HCCT-2010, ozone concentrations were measured at all three measurement sites with high time resolution using TE49C-TL (up-/downwind sites) and APOA360 (summit site) gas monitors. The measured concentrations are presented in Section 3. Previous studies have shown (*e.g*. Wilson and Birks, 2006) that ozone measurements by UV absorption*, i.e*. those obtained using a TE49C analyser, can be influenced by potentially large water vapour interferences. In the present studies, the air was not dried before measuring ozone concentrations with the gas monitors. Since the impact on the obtained concentrations should be quite similar for all three sites (similar high relative humidity at all three sites), the temporal behaviour of the measured time series should be not much affected by this artifact. However, for other studies, the influence of water vapour on measured ozone concentrations should be considered.

A connected flow analysis based on measured ozone concentrations comprises a comparison of the concentration time series measured at each site with regard to the concurrency of the ozone concentration levels as well as their temporal behaviour and dependency on the local meteorological conditions. In order to obtain an overall comparison of the concentration time series at the three measurement sites and to investigate the flow connectivity in detail, the CODs for each of the three sites were also calculated using the measured ozone data. Here, low COD values indicate a good concurrency of the ozone concentration time series measured

at a given two sites. For a COD calculation at a given time, measured ozone concentrations of a 1 hour time interval were used time-centred around the specific time point. The ozone CODs calculated in this manner are presented in Section 3 and given in table form in the ESM. As was the case for the particle measurements described in the previous section, no time lag between the time series associated with the three measurement sites was applied in these COD calculations.

Since the time lag between the measurements, which is mostly correlated with wind speed, was not considered in the present COD analysis and the pattern of the concentration time series are less important for COD analysis, another statistical measure, the cross-correlation value r_{xcor}, was also used to assist in the characterisation of the flow connectivity between the different sites. This measure can be used to compare two time series that cover the same time span: for two time series x and y, the cross-correlation value at lag time d is defined by

$$r_{xcor}(d) = \frac{\sum_i \left(\left[x_i - \bar{x} \right] \cdot \left[y_{i-d} - \bar{y} \right] \right)}{\sqrt{\sum_i \left[x_i - \bar{x} \right]^2} \cdot \sqrt{\sum_i \left[y_{i-d} - \bar{y} \right]^2}} \qquad (2)$$

As can be seen from Eq. 2, the calculated value of r_{xcor} depends on the magnitude of the time lag between the two time series. The time lag with the highest r_{xcor} value provides an indication of the air parcel transport time between a set of two stations. High correlations between the measured concentration profiles indicate the existence of connected flow between the three sites and the absence of substantial mixing with surrounding air during air parcel advection. The calculated r_{xcor} are presented in the ESM for selected time periods during each of the FCEs identified during the measurement period.

The cross-correlation analysis presented in this section was also performed for the particle data described in the previous section. However, since the temporal resolution of the particle data was coarser than that of the ozone data, and the magnitude of temporal variation in N_{49nm} was smaller than that observed for measured ozone concentrations, cross-correlation analysis of the N_{49nm} data did not yield additional useful information. For this reason, the results of this analysis are not considered in the present paper.

2.4 Characterisation of the flow conditions with non-dimensional parameters

Non-dimensional flow and stability parameters such as the Froude number (Fr) and the Richardson number (Ri) can be used to characterise the flow regime in mountainous terrain. Advantageously, such parameters do not require numerically expensive models but rather can be easily derived from locally measured meteorological data. In the literature, the term "Fr number" is used to describe a variety of quantities, each of which have dissimilar forms and dynamical significance (see Baines, 1995 for details). In the present paper, the Fr number is defined as in Pierrehumbert and Wyman (1985)

$$Fr = \frac{NH}{U} \tag{3}$$

in order to characterise whether an air mass will be lifted up and pass over, or be forced to stream around, a mountain barrier. As can be seen from Eq. 3, the Fr number represents the ratio of the atmospheric potential energy, which is related to the product of the Brunt-Väisälä frequency N and the maximum mountain height H, to the kinetic energy of the air flow, which is represented by the characteristic wind speed U of the incoming air flow. The direct proportionality of the Fr number to the atmospheric stratification represented by the Brunt-Väisälä frequency implies that under stable stratification conditions of the boundary layer, the Froude number tends to larger values for a given wind velocity. Higher Fr numbers, which exist under highly stable stratified conditions and/or low wind speeds, reflect the existence of blocking effects.

Model simulations by Pierrehumbert and Wyman (1985) have revealed three critical Froude numbers. For Fr > 0.75, a disturbance propagates upstream with time and results in a decelerated low-level flow, where gravity waves start to amplify. Under these conditions (*i.e.* under decelerated or blocked upwind low-level flow conditions), stronger downdrafts behind the mountain ridge can occur. These downwind site downdrafts lead to a mixing of low-level air with air from higher altitudes (see Pierrehumbert and Wyman, 1985). For Fr ≥ 1.5, the simulations predict the occurrence of a stagnant area at the low upstream slope. Simulations with even larger Fr numbers (Fr > 2) predict the existence of a fully blocked flow pattern with a stagnant area at the upstream slope. As Fr continues to increase, this stagnant area extends further in the vertical direction. These theoretical findings have been validated by both laboratory experiments (Baines, 1995) and tracer studies (Bruintjes et al., 1995; Vosper et al., 2002).

The Fr formulation described above assumes a dry adiabatic lifting of the airflow. However, studies by Jiang (2003) and Colle (2004) have revealed that the critical Fr number (*i.e.* the value at which the stagnation pattern initiates) is 30–100% higher in cases where cloud formation—and associated release of latent heat—occurs. However, since there are many uncertainties associated with the determination of the magnitude of latent heat release from cloud formation, only the "dry" Froude number is used in the present work.

Another dimensionless parameter characterising the level of atmospheric stratification with respect to blocking effects is the Richardson number (Ri), which reflects the ratio of the energy extracted by buoyancy forces to the energy gained from wind shear:

$$Ri = \frac{g \, \partial\theta / \partial z}{\theta \left(\partial U / \partial z \right)^2} \tag{4}$$

Eq. 4 includes vertical gradients $\partial / \partial z$ of both the potential temperature θ and the characteristic wind speed U; in this equation, g represents the gravitational acceleration. The sign of the Richardson number reflects the extent of thermal stratification: for Ri > 0, the airflow is statically stable; for Ri < 0, the airflow is statically unstable; for Ri = 0, the airflow is neutral. Under statically stable conditions, airflow will become dynamically unstable for Ri numbers below a critical value of ~0.25.

For HCCT-2010, the characteristic non-dimensional flow and stability parameters Fr and Ri were calculated using rawinsonde data from the German Weather Service Station in Meiningen (453 m amsl, provided by the University of Wyoming, http://weather.uwyo.edu/upperair/sounding.html), which is located ~30 km upwind of Mt. Schmücke. Average values and vertical gradients of U and θ were determined by averaging measurements obtained at the Meiningen station. An effective mountain height of 484 m was used for the Fr and Ri calculations, since this height is broadly representative of the mountain ridge level in this region. The Fr and Ri numbers calculated in this manner are given in Section 3.

Finally, it should be noted that since the calculation of Fr and Ri numbers is based in part on data taken ~30 km upwind of Mt. Schmücke, it therefore assumes that both the wind conditions and the thermal stratification were conserved during transport to the measurement

site. Since this assumption may not always be valid, the calculated values of Fr and Ri should be used with caution.

2.5 Tracer experiments

To study the local air flow under appropriate meteorological conditions, four tracer experiments (TE) were performed during the campaign (see Table 1). In these experiments, sulphur hexafluoride (SF_6) was used as an inert tracer gas and released from a point source (bottle) at the upwind site Goldlauter at a rate of ~3 L min^{-1} for 10–20 min . Air samples were then taken at 8 different sites along the expected air flow, including the Mt. Schmücke summit and the downwind Gehlberg sampling sites. The locations of the sampling sites are indicated in Fig. 2 and given with geographical coordinates in Table S1 (ESM). Their selection was based on the choice of sites during the previous FEBUKO experiments (Heinold et al., 2005). For consistency, the ID numbers assigned to the sites were kept the same as in Heinold et al. (2005). Air sampling at the sites commenced at the start of the SF_6 release and was performed at 5-minute intervals over the course of one hour.

Each sample was collected in a 10 L polyethylene bag, which was exposed to ambient air for 5 seconds, firmly closed, and transported to the laboratory within 24 hours of sampling. Analysis of SF_6 was performed using gas chromatography (GC) with electron capture detection (ECD) using a Siemens Sichromat 1-4 system. A defined amount of air was removed from each bag with a gas-tight syringe and directly injected into the GC. The detection limit of the GC method employed, which is described in detail elsewhere (Strunk et al., 2000), was 0.5 ppt and the precision was < 1 %.

2.6 Detailed characterisation of the meteorological and microphysical conditions

For the examination of the local meteorological conditions during the selected FCE periods, locally measured meteorological and microphysical data, rawinsonde observations, satellite pictures, ceilometer data and calculated backward trajectories were used. Our examination focused on the stability of the incident flow conditions, synoptic front passages, the presence of orographic or non-orographic cloudiness, measured cloud properties such as cloud base height and LWC, vertical thermal stratification, and precipitation.

For detection of frontal processes and synoptic-scale advection patterns, surface weather charts with a time resolution of 6 hours and charts of the 850 hPa pressure level were used (see the ESM). In order to identify the air mass origin and to characterise potential source regions of the aerosols measured during a FCE, backward trajectories were calculated with the HYSPLIT model (Draxler and Rolph, 2003; Rolph, 2013). The HYSPLIT model was used in the ensemble mode in order to provide multiple backward trajectories based on a small variation in the applied initial meteorological field. Ensemble trajectory calculations were performed to lower the uncertainties associated with a single trajectory and to investigate the potential variability of the calculated backward trajectories according to variations in the meteorological field. Each calculated ensemble trajectory started from the same location; however, in each case the initial meteorological field was offset by 1 grid cell in the horizontal and by 250 m in the vertical direction. In this manner, 27 ensemble backward trajectories were calculated (see the ESM for further details). In order to gain more information regarding aerosol type and origin, the trajectories were also characterized with respect to their residence time over certain land types (urban, agriculture, natural vegetation and bare areas) or water areas during their transport to Mt. Schmücke (see van Pinxteren et al., 2010 for details of the trajectory analysis approach).

For the characterisation of cloud conditions and thermal stratification, satellite pictures and rawinsonde observations were used. For the analyses, both IR and VIS satellite pictures obtained by the geostationary METEOSAT satellite (with 15 min time resolution) and, if available during the FCEs, polar orbit satellite pictures (obtained from Berliner Wetterkarte e.V., 2010 and DLR) were examined. As discussed in Section 2.4, information regarding tropospheric thermal stratification and vertical wind pattern was obtained from analysis of rawinsonde observations from the German Weather Service station Meiningen (source: http://weather.uwyo.edu/upperair/sounding.html). Vertical wind pattern data in particular was used to characterise vertical thermodynamic conditions for existing clouds, which allowed for the determination of the cloud type present at the measurement site.

Standard meteorological parameters such as temperature, pressure, relative humidity, wind direction, wind speed and precipitation were measured at all three measurement sites using Vantage Pro weather stations. Cloud base height was measured at the upwind site using a ceilometer (Jenoptic Ceilometer CHM 15k) and LWC was measured at the summit site using two instruments (FSSP-100 and PVM-100); these data were used to characterise the local

microphysical cloud conditions and their temporal homogeneity throughout each FCE. The locally measured data also helped to enable the detection of meteorological front passages and, by extension, possible air mass changes. Overall, the meteorological analysis described in this section allowed for a more sophisticated and comprehensive evaluation of the suitability of selected cloud periods for further analysis using a Lagrangian-type approach.

2.7 Characterisation of the regional flow conditions using COSMO

For the model-based investigation of the flow conditions, simulations with the meteorological forecast model COSMO (Baldauf et al., 2011; Schättler et al., 2012) were conducted for the whole measurement period. In brief, COSMO is based on the primitive hydro-thermodynamical equations that describe compressible non-hydrostatic flow in a moist atmosphere. It uses a staggered Arakawa C-grid on a rotated geographical coordinate system and a hybrid terrain-following vertical coordinate. The COSMO model includes the dynamic kernel for the atmosphere and the required parameterisation schemes for numerous meteorological processes, boundary conditions and surface exchange relations. COSMO can describe not only the atmospheric flow but also phenomena occurring between the meso- and micro-scales, including near-surface processes, convection, clouds, precipitation, orographic and thermal wind systems. Further details on the model and its implementation can be found elsewhere in the literature (see *e.g.* Baldauf et al. (2011)). In the present study, the COSMO model was applied for a domain spanning between 50°N, 9.5°W and 51°N, 11.5°W with a horizontal resolution of ~1.4 km (100 × 80 grid cells). For the investigation of the regional-scale flow conditions, the wind field predicted by COSMO was used. The model output is presented in the ESM for each of the FCEs identified during the measurement period.

3 Results and discussion

3.1 Characterisation of the general synoptic situations and advected air masses during HCCT-2010

As shown in Fig. 3, the average synoptic situation during September 2010 was characterised by a weak low-pressure area between Greenland and Iceland as well as a weak high-pressure area over Romania, which together resulted in a predominantly westerly flow over Central

Europe. The second half of the month in particular was affected by front passages and variable weather conditions.

At the beginning of the field campaign on September 14, at the foreside of a trough over Central Europe (TM), marine air from North Atlantic (mTp) was advected to the measurement site. The day after, the trough moved eastwards and an Atlantic frontal zone reached Central Europe, which led to precipitation with occasional gusty winds. On the backside of the cold front, Greenlandic polar air (mP) was advected to the Mt. Schmücke area; this air mass stayed until September 17. Trajectory analysis showed that this air mass was mainly influenced by marine and agricultural areas of Great Britain or France. Given the presence of appropriate wind conditions, several (some quite short) offline measurement periods were conducted during this period, despite the presence of precipitation (see Table 2). From September 18 onward, a bridge of high pressure developed over Central Europe. Warmed maritime polar air (mPt) with decreasing oceanic influence approached the Thuringian Forest over the course of the following week (until September 23), which resulted in moderate winds, mainly from the SW. On September 20 and 21, the wind direction shifted towards easterly directions without any change in the origin of the air mass. This is in agreement with the trajectory analysis for this period (see the ESM), which showed that the influence of the continent (*i.e.* agriculture, natural vegetation) on the air mass increased dramatically with time over the week. On September 24, a transition occurred, and the air mass advection changed towards a more polar air mass. Over the next three days (until September 28), a strengthening low-pressure area over the North Sea advected aged Greenlandic polar air (mP) to Central Europe. The weather conditions were appropriate for another offline experiment period on September 24 and 25 (see Table 2). The weather situation thereafter was characterised by strong precipitation, which was connected to front passages. The weather situation from September 29 to October 3 was affected by a large high-pressure system over Scandinavia and a low-pressure system over Iceland, which generated temporary precipitation at the corresponding fronts. The air mass was characterised by drier and warmer air (cTp) as compared to previous days and by advection over the continent (France) from the SW. Two offline experiment periods were conducted during this weather situation (see Table 2).

As shown in Table 2, October 2010 experienced 5 distinct weather periods. No change in the general weather situation was observed for the first three days of October as compared to the

last period in September. As stated above, two offline experiment periods were conducted during this weather situation. The weather situation from October 4 to October 8 was characterised by a high-pressure area over Russia and Poland and areas of low pressure over the Atlantic Ocean. The Mt. Schmücke area in particular was in a zone of weak pressure gradients characterised by warm and humid air advected from the Mediterranean area in the south. The declining pressure gradients caused weak winds first from the SW and later, from October 6 onward, from different directions. One offline experiment period were conducted during this weather situation (see Table 2). The marine-influenced tropical air mass (mTs) caused early morning fog in the Mt. Schmücke area but precipitation only in Southern Germany. Frontal systems were blocked in the west and south of Germany by the high-pressure area over Poland and Russia. By October 9, the weather situation changed: the high-pressure area over Poland and Russia receded and a new high-pressure area formed over the Norwegian Sea (HNA); in addition, the wind changed to northerly directions, which advected dry continental polar air masses (cP). At this time, under the influence of high pressure, the Mt. Schmücke area experienced early morning fog. Pressure gradients were still weak. By October 15, the general weather situation started to change; from October 16 onward, a trough area over Central Europe (TrM) influenced Mt. Schmücke. The trough led to an advection of humid marine polar air masses (mP), which were associated with occasional precipitation over Germany. Two offline experiment periods were conducted during this time period (see Table 2). From October 22 onward, the trough was pushed eastward and westerly conditions (WZ) affected the Mt. Schmücke area, which advected marine air masses (mPa). During this weather situation, two offline cloud experiments were performed (see Table 2).

3.2 Flow characterisation

3.2.1 Overflow characterisation with the quasi-inert tracer O_3

As discussed in Section 2, measured ozone concentration time series and derived statistical parameters such as the COD and the cross-correlation can be used for the characterisation of the flow connectivity between the different measurement sites and, by extension, for the identification of suitable experimental periods for further investigations. The ozone concentration time series at the three measurement sites and the calculated COD values based on these time series are presented in Fig. 4, together with important meteorological data such as wind speed and direction. Briefly, it is noted that the meteorological measurements at the

upwind site Goldlauter were performed in a rather narrow valley, *i.e.* under less suitable wind measurement conditions, and for this reason the wind data obtained at this site should be used with great care only.

Fig. 4 shows that the ozone concentrations at the different sites displayed significant spatial and temporal variation—this short-range variability represents the precondition for the statistical analysis. During the measurement period, the ozone concentrations at the three sites varied between several ppb and ~60 ppb. As shown in Fig. 4, ozone concentrations measured at the summit and downwind sites generally agreed quite well; by contrast, concentrations measured at the upwind site often deviated from those measured at the other two sites. Strong agreement, and therefore good flow connectivity, between the three ozone concentration time series was mostly present during weather situations with south-western or west-south-western flow conditions. Strong agreement was also present during weather situations with north-eastern winds perpendicular to the mountain ridge. Fig. 4 also shows that periods of measurement agreement were associated with higher wind speeds. This congruence reflects the higher kinetic energy of the airflow and, therefore, the higher probability for the air to cross the mountain range. In Fig. 4, the time intervals displaying the highest congruence are highlighted as shaded areas.

Comparison of the measured concentration-time profiles with the associated calculated CODs shows that larger concentration deviations between the time series coincide directly with higher CODs. The COD analysis reveals that higher CODs are typically observed for the upwind site; indeed, the average of the $COD_{GB\text{-}SM}$ (0.11) throughout the analysis period is smaller than those of the other two site combinations ($COD_{SM\text{-}GL}$ = 0.13; $COD_{GB\text{-}GL}$ = 0.16). This result is in agreement with the time series measurements discussed above, which generally found stronger correlations between ozone concentrations at the summit and downwind measurement sites.

High COD values arise not only during periods of low wind speed but also during periods of high vertical thermal stratification. During one such period, which was observed from September 18–25, nighttime ozone concentrations at the upwind valley site Goldlauter were often 15–30 ppb lower than those measured at the other two stations (see Fig. 4). A difference of this magnitude cannot be explained by short-term interactions with local emissions, lowered production, and deposition only. Analysis of rawinsonde data during this time period shows distinct low-level nighttime inversions, which suggests that air exchange did not occur

during this time. Under such conditions, local emission *(e.g.* of NO into the near-ground inversion layer) and deposition processes could result in strongly lowered ozone concentrations. Support for this interpretation is provided by the fact that ozone concentrations at the upwind site largely paralleled those at the other two measurement sites during daytime, when inversions were not present. Disconnected flow was not always observed under nighttime conditions, however: on the night of September 23–24, for example, the ozone concentration measured at the upwind site was substantially different from those measured at the other two stations in the evening of September 23 and the early morning hours of September 24; at midnight, however, the three concentrations were similar. It is likely that the inversion was not present at this time. In summary, nighttime inversion conditions led to the disconnection of the upwind valley site from the two downwind sites, and this disconnection is reflected in differences in the ozone concentration time series measured at this site. These differences are also reflected in the high COD values observed for this site under these conditions, which in turn indicate that connected airflow did not occur during inversion periods. Taken together, therefore, the COD values and the ozone concentration time series provide an excellent indication of the extent of local flow connectivity.

A histogram of the ozone CODs for the different measurement site combinations is provided in Fig. 5. As shown in this figure, a higher number of smaller CODs are calculated for the summit/downwind site combination ($COD_{GB\text{-}SM}$): more than 60% of the ozone CODs (GE/GL) at this site are smaller than 0.15. This observation reflects the largely more correlated ozone time series at these two locations as compared to the two location pairs that include the upwind site.

Further investigation of the three ozone concentration time series revealed good congruencies between the three measurement sites for CODs ≤ 0.1 and acceptable congruencies for CODs ≤ 0.15. For larger CODs, by contrast, large deviations between the three time series were observed, which suggests that the flow between the field sites was disconnected. Based on these findings, the ozone COD dataset was used to conduct a qualitative assessment of the conditions during the campaign and to identify suitable and unsuitable time periods for further analysis. Calculated COD values were subject to the following classification scheme: (1) $COD \leq 0.05$ (very good correlation), (2) $0.05 \leq COD \leq 0.1$ (good correlation), (3) $0.1 \leq COD \leq 0.15$ (slight correlation), (4) $0.15 \leq COD \leq 0.2$ (poor correlation) and (5)

$0.2 \leq$ COD (very poor or no correlation). The results of the overall assessment of the flow connectivity, which included consideration of other parameters, are summarised in Table 5.

The results of cross-correlation analyses performed using the ozone concentration profiles at the three measurement sites were similar to those obtained from the COD analyses. The cross-correlation plots for each identified FCEs are presented in the ESM. A representative cross-correlation plot (from the FCE1.1) is presented in Fig. 5. As shown in this figure, high cross-correlations (r_{xcor} ~0.7–0.9) were present during this time period, which suggests the existence of high flow connectivity between the three sites. The highest cross-correlations were present between 0 and -20 min time lags. This finding implies that, during this time period, the mean air transit time between sites (*e.g.* from the summit to the downwind site; green line in Fig. 5) was ~10 min and the overall mean transit time between upwind and downwind sites was ~20 min. As was observed in the COD analysis, the correlations between the summit and the downwind sites were usually somewhat higher than correlations observed for site combinations including the upwind site. It should be noted that transit times can vary considerably on the timescale of a FCE period. Therefore, the ESM includes cross-correlation plots not only for the entire duration of each period but also for shorter time intervals (typically 3 hours) during each period. The results of the cross-correlation analyses for each of the FCEs selected for overall assessment are summarised in Table 5.

3.2.2 Overflow characterisation with aerosol particle distribution data

In addition to the ozone concentration measurements described in the previous section, particle number concentrations from the 49 nm (N_{49nm}) and 217 nm (N_{217nm}) size bins of the SMPS were used for the assessment of flow connectivity between the three measurement sites and the assessment of prevailing cloud conditions. The measured particle number concentrations at the three sites and the corresponding three COD values are presented in Fig. 4. This data clearly shows that the N_{49nm} and N_{217nm} values at the different sites are variable, and therefore that they are suitable for use in COD analysis.

For the most part, the N_{217nm} plot shows quite good agreement between the measured data obtained at the upwind and downwind sites. Number concentrations (N_{217nm}) obtained at the summit site, by contrast, show larger differences under some conditions. As can be seen from the plot, the N_{217nm} bin always shows very low concentrations in the presence of clouds or fogs, which is attributable to CCN activation in this size range. This behaviour leads to large

COD values ($COD_{N217nm} > 0.8$) during cloud conditions at the summit site and non-cloud conditions in the upwind and downwind valleys.

For this reason, the N_{217nm} parameter can be used—in addition to measurements of liquid water content at Mt. Schmücke—to characterize cloud/fog conditions at the measurement sites and to distinguish between flow conditions with and without cloud interaction. In order to separate time intervals with clouds from those without clouds (*i.e.* with/without activation of accumulation mode particles), a critical COD_{N217nm} value was defined: for $COD_{N217nm} > 0.4$, activation of accumulation mode particles is expected and thus cloud conditions are assumed to have been present at the summit site.

Unlike the N_{217nm} plot, the N_{49nm} plot shows quite good agreement between the measured data obtained at all three measurement sites. The calculated COD_{N49nm} shows the lowest values during weather situations with both SW and NE winds, which indicates that good flow connectivity exists under these conditions. Comparison of the N_{49nm} time series with the corresponding calculated COD_{N49nm} values shows that larger deviations between measured concentration profiles coincide directly with higher COD_{N49nm} values. While COD_{N49nm} values generally paralleled COD_{O3} values, the COD_{N49nm} time series typically exhibited more noise. This enhanced noise most likely arose as a result of the coarser time resolution of the particle concentration input data and the overall lower variability in COD_{N49nm} values as compared to COD_{O3} values.

Overall, examination of the N_{49nm} temporal profiles revealed that reasonable congruencies between the three profiles existed for $COD_{N49nm} \leq 0.2$. For larger COD_{N49nm} values, larger deviations were present, which suggests that a disconnection of the flow between the three field sites most likely existed. Based on this finding, and those obtained in previous studies (see Section 2), the COD_{N49nm} dataset was used to conduct a qualitative assessment of the conditions during the campaign and to identify time periods with and without connected flow conditions. Calculated COD values were subject to the following classification scheme: (1) $COD_{N49nm} \leq 0.05$ (very good correlation), (2) $0.05 \leq COD_{N49nm} \leq 0.1$ (good correlation), (3) $0.1 \leq COD_{N49nm} \leq 0.15$ (satisfactory correlation), (4) $0.15 \leq COD_{N49nm} \leq 0.2$ (slight correlation) and (5) for $0.2 \leq COD_{N49nm}$ (very poor or no correlation). The COD_{N49nm} dataset was then colour-coded according to cloud conditions and to the above classifications of connected flow conditions (see the ESM). These results were used in the selection of the most suitable periods for further investigation (see Section 3.2.3). The results of the overall

assessment of the flow connectivity, which included consideration of other parameters, are summarised in Table 5.

3.2.3 Selection of potentially suitable investigation periods

The main goal of the present study was to quantitatively and objectively identify periods of time during the HCCT-2010 campaign when the three measurement sites experienced connected flow conditions. Full-cloud events (FCEs), which we define as time periods with connected SW flow conditions and cloud conditions present only at the Mt. Schmücke summit site, and non-cloud events (NCEs), which we define as periods with connected SW or NE flow conditions and no clouds/fog at any site, were identified according to the two-step procedure shown in Fig. 6.

According to this procedure, periods with connected flow condition (SW/NE wind sector) were first identified according to the flow criteria described previously. Then, the measured LWC at the Mt. Schmücke site was used to evaluate the cloud conditions, and the CODs of the aerosol number concentration (N_{217nm}, activated CCN bin under typical cloud/fog conditions) were used both to identify cloud/non-cloud conditions at the summit and to exclude conditions with fog at the valley sites. Finally, only periods with insignificant amounts of precipitation (RR: precipitation rate during the last 30 min) at each of the three sites were selected. The entire dataset, including meteorological data, calculated CODs, and a table describing the identified FCEs and NCEs, is given in the ESM. A brief summary of the most important parameters associated with each of the selected FCEs is given in Table 3. The final evaluation of all of the FCEs is summarised in Table 5.

The name associated with each of the identified FCEs reflects their chronological occurrence during HCCT-2010. Periods of prolonged cloud presence, which could also include small cloud-free breaks (*i.e.* conditions with LWC values close to zero), were determined based on the LWC time series measured at Mt. Schmücke and numbered chronologically. Each defined cloud period was further subdivided into individual uninterrupted cloud event periods *(i.e.* continuous cloud conditions, without very low LWC values). For example, the event FCE1.1 refers to the first (uninterrupted) part of the first prolonged cloud period that occurred at Mt. Schmücke during the experiment.

3.3 Overflow characterisation with non-dimensional parameters

The calculated Froude (Fr) and Richardson (Ri) numbers for the different rawinsonde observations (from Meiningen, which is located ~30 km upwind of Mt. Schmücke) during or near the selected FCEs/NCEs (with SW flow conditions only), as well as associated remarks are listed in Table 4. Since the focus of the present study is the FCEs, only the Fr and Ri numbers related to the FCEs are discussed here in detail.

As can be seen from Table 4, the Fr number predicts a stagnant flow/area during only a few FCEs; during the majority of the identified FCEs, no blocking or only a slightly decelerated flow was present. The calculated values show that the flow conditions were largely determined by the extent of atmospheric stratification and, in some cases, by the wind speed conditions. Large Fr numbers coincided always with large Ri numbers, which indicated very statically stable conditions. Under these stable conditions, however, acceptable flow conditions could still be achieved: on September 14 (14:00 CEST), for example, high mean wind speeds (8 m s^{-1}) allowed for air flow over the mountain ridge.

These non-dimensional parameters compare well with the calculated COD values for ozone and the N_{49nm} size bin (COD between the up and downwind site): higher Fr and higher Ri numbers, which indicate a potential blocking of the airflow, generally coincide with higher COD values, which reflect deviations between the different sites.

During FCE 11.3, for example, the Fr number on October 2 (14:00 CEST) was 0.81, which indicates that airflow over the mountain range was possible; by the early morning hours of October 3 (2:00 CEST), however, the calculated Fr (1.31) and Ri (7.19) numbers imply a stronger deceleration of the flow under very stable conditions. This latter result is confirmed by the ozone COD analysis, which revealed CODs > 0.2 after 00:30 (CEST). Similar results were obtained during FCE 13.3, in which better flow conditions are predicted by the Fr number during the daytime (14:00 CEST) on October 6 ($Fr = 0.85$; $COD_{O3} = 0.09$; $COD_{N49nm} = 0.12$) than during the subsequent nighttime (02:00 CEST) observation on October 7 ($Fr = 1.16$; $COD_{O3} = 0.14$; $COD_{N49nm} = 0.27$). During this latter period, a disconnection of the upwind site from the two other sites appeared to be present after 01:00 CEST (see Table 4 and the time-resolved COD analysis data in the ESM).

3.4 Detailed meteorological characterisation of the identified FCEs

Meteorological conditions, including the separation of orographic and non-orographic clouds, the detection of frontal processes, the stability of air mass advection (local/synoptic scale) and the cloud conditions (LWC, precipitation, cloud base height), were examined in detail for each of the identified FCEs. These data were obtained from locally measured meteorological and microphysical data, rawinsonde observations, satellite pictures, ceilometer data, and calculated backward trajectories. For reasons of clarity, all detailed information for each FCE is given in the ESM.

3.5 Model-based characterisation of the flow conditions during FCEs

The extent to which the identified FCEs met the required overflow conditions was also characterized using the wind field predictions of the COSMO model. Figures showing the horizontal wind conditions predicted by the COSMO model in the Mt. Schmücke area for each of the selected FCEs are presented in the ESM.

A nearly constant wind field, with wind arrows of approximately the same orientation (SW) and length *(i.e*. the same wind speed and direction) is a good indication for mountain overflow conditions without a deceleration/blocking of the flow, without significant downward mixing of air from higher levels, and without a circulation around the Thuringian Forest. This condition was fulfilled for all FCEs during September and for FCE26.1/FCE26.2 in October, in which very constant SW flow conditions were predicted by COSMO. For example, as illustrated in Fig. 7, FCE7.1 showed a very homogeneous regional wind field with similar wind directions and wind speeds before, on top and behind the mountain ridge, which indicates an adequate flow over the mountain (*i.e.* without an upwind deceleration of the incoming flow and almost no entrainment of higher-level air).

The other FCEs (11.2, 11.3, 13.3 (in part), 22.0 (in part), 22.1, and 24.0), by contrast, showed less congruent wind directions and wind speeds before, on top and behind the mountain ridge—for these FCEs, the COSMO model predicted an upwind blocking, at least in part. For example, as shown in Fig. 7, the model predicted decelerated flow conditions in the upwind area and stronger winds in the downwind area during FCE 24.0. The latter prediction indicates the presence of downdrafts in the lee of the mountain ridge and, thus, entrainment of air from higher altitudes.

The COSMO-predicted wind conditions during each of the identified FCEs are presented in Table 5. In general, these modelled results are quite consistent with the results obtained from the COD and cross-correlation analyses discussed previously. Therefore, the connected flow validation scheme developed in this work is approved to be applicable for identifying suitable flow conditions for a hill cap cloud experiment.

3.6 Tracer experiments

Four SF_6 tracer experiments (TE) were carried out during the HCCT-2010 campaign (TE1–TE4; see Table 1). Although all of these experiments were carried out when local meteorological conditions seemed favourable, post-campaign COD analysis of flow connectivity between the three measurement sites revealed that only two of the experiments (TE 1 and 3; see ESM) were conducted under connected flow conditions suitable for Lagrangian-type comparisons of concentrations at upwind and downwind sites. TE 1 was conducted during the NCE0.4 period, while TE 3 was conducted during the FCE13.3 period. By contrast, COD analysis indicated that the other two experiments (TE 2 and TE 4) were performed under conditions of poor flow connectivity between the sites. For this reason, only the results obtained during TE 1 and TE 3 are shown in Fig. 8.

Different plume pathways were observed during TE 1 and TE 3, which reflects differences in the dominant wind direction during these experiments. The mean wind direction at the Mt. Schmücke summit site (dd_{SM}, 20) had a higher westerly component during TE 1 (mean dd_{SM} of 240°, cf. Table 1) than during TE 3 (mean dd_{SM} of 220°). As a result, the TE 1 plume passed closer to the sampling sites to the east of the release site (22, 44, and 32) than those to the west of the release site (21, 41, and 30). The opposite was observed during TE 3: higher SF_6 mixing ratios were observed at the western sites (41 and 30). Although somewhat lower SF_6 mixing ratios were observed at the western site 21 than at its eastern counterpart site 22, peak SF_6 concentrations at site 22 were reached later than at the Mt. Schmücke site (20), which is further downwind. This indicates that site 22 was likely not part of the main pathway of the plume.

During both TE 1 and 3, the highest SF_6 mixing ratios (~110 ppt) were usually observed at the Mt. Schmücke site. As a result of diffusion and dilution, lower mixing ratios were observed at the downwind sites. However, SF_6 concentrations at these sites (30–60 ppt) were still well

above background levels, which provides support for the assumption that connected air flow between the upwind, summit, and downwind sites was present during these experiments.

Although the SF_6 plume did not directly pass the Gehlberg downwind site (30) during TE 3, it did, however, pass the nearby Am Brand downwind site (32). It seems valid, therefore, to assume that during the FCEs (and NCEs), where a spatially more homogeneous aerosol population was transported through the area (*i.e.* rather than a plume originating from a point source), representative air parcels were able to be sampled at the Gehlberg site (30), as long as a SW flow was present.

The SF_6 transit time—here defined as the time difference between its initial release and the measurement of the maximum mixing ratio at one of the two downwind sites (30 or 32)—was 30 min for TE 1 and 45 min for TE 3. The mean wind speed at the Schmücke site during TE 1 was about twice as high as that measured during TE 3, which provides qualitative support for the faster transit time observed during TE 1. It should be noted that in both experiments the measured transit time also included the time required for SF_6 to diffuse from the ground to higher altitudes, where it then could be transported with higher wind speeds. Since the upwind site is located close to the ground and in a rather narrow valley, the wind speed at this location was always significantly lower than at Mt. Schmücke (< 1 m s^{-1} during both TE 1 and 3). The transit times observed during the SF_6 tracer experiments are thus expected to be somewhat longer than those of "representative" air parcels during FCEs, since these parcels did not arise from a point source on the ground but rather traveled with the higher wind speeds above the ground.

Experimental results for the TE 2 and TE 4 tracer experiments are shown in Figures S5 and S6 in the ESM. Much lower SF_6 mixing ratios were observed at the Mt. Schmücke summit (20) and at the downwind sites 30 and 32 during TE 2 than during TE 1 and 3, which indicates either that the SF_6 plume did indeed not directly pass these sites or that vertical lifting from the upwind site was blocked. During TE 4, no increase in SF_6 mixing ratios was observed for the first 40 min after the initial SF_6 release, even at the sites closest to the upwind site (21 and 22), which indicates a strong decoupling/blocking of the upwind site. This finding is supported by the flow connectivity analysis performed for this time period (see the ESM). Together, these results confirm that flow connectivity between the measurement sites was not present during TE 2 and TE 4.

Overall, the SF_6 tracer experiments serve as empirical support for two crucial assumptions/prerequisites of the HCCT-2010 campaign: i) under appropriate meteorological conditions a Lagrangian-type analysis of experimental data is valid and ii) the flow validation scheme developed in this work is suitable for identifying such conditions.

3.7 Overall evaluation of the FCEs

A comprehensive assessment of the meteorological and flow conditions during the ground-based cloud passage campaign HCCT-2010 has been used to conclusively verify that the selected FCEs meet the required conditions for a Lagrangian-type experiment. The results of this assessment, including the advantages and disadvantages of each individual FCE, are outlined in Table 5. This table also includes an overall conclusive statement regarding the suitability of the meteorological and flow connectivity conditions during each FCE.

It can be qualitatively concluded from Table 5 that the meteorological and flow connectivity conditions during the 14 FCEs largely fulfilled the requirements associated with the Lagrangian-type experiment performed during HCCT-2010. Since each FCE has unique advantages and disadvantages, however, no final ranking of the FCEs was performed. Furthermore, it is necessary to keep disadvantages of some FCEs, such as occurred precipitation, in mind. Some disadvantages might be needed for further investigations and interpretations of other measurement data. Despite these disadvantages, however, all FCEs and NCEs identified in the present study are recommended for use in further investigations of the HCCT-2010 dataset.

4 Summary

The main goal of the present study was to provide a comprehensive evaluation of the meteorological and connected flow conditions present during the ground-based Lagrangian-type experiment HCCT-2010, in order to provide a set of suitable measurement time periods for detailed investigations (see e.g., Harris et al. 2013, 2014, Spiegel et al. 2012). In order to accomplish this goal, synoptic and local scale advection conditions during HCCT-2010 were examined and classified. The local flow conditions throughout the entire measurement period were studied by means of statistical analyses and corresponding statistical measures (COD and cross-correlation). In particular, the particle number concentrations in specific aerosol

size bins and the concentrations of the quasi-inert trace gas ozone at the upwind, summit and downwind sites were used for the statistical analyses.

The entire HCCT-2010 measurement period was analysed with respect to flow connectivity between the three measurement sites and the presence or non-presence of a cloud at the sites. For further verification of the local flow connectivity and improved understanding of local air transport processes in the experimental area, tracer experiments were conducted using the inert gas SF_6. Then, full-cloud events (FCEs) and non-cloud events (NCEs) were identified in an objective manner according to a set of developed flow and precipitation criteria. The mesoscale airflow over the mountain ridge during the identified FCEs and NCEs was characterised by means of the non-dimensional parameters Fr and Ri, which were calculated from rawinsonde observation data. In addition, the local meteorological conditions during the identified FCEs were studied in detail. Simulations performed using the weather forecast model COSMO were used to further investigate the regional and local flow conditions. These simulations enabled the characterisation of the regional wind pattern and the identification of decelerated or blocked flow conditions at the upwind site and downdrafts at the downwind site.

This comprehensive examination showed that orographic cloudiness was most often observed for SW weather type situations with stable incoming flow. In total, approximately one third of the examined HCCT-2010 cloud periods were characterised by orographic cloudiness; the other two thirds were characterised by clouds associated with synoptic fronts. The results of the statistical flow analyses and SF_6 tracer experiments performed in this study show that a strong link between the three measurement sites exists, particularly under constant SW flow, high wind speed and slightly stable stratification conditions. The findings of the COD and cross-correlation analysis were supported by results obtained from regional modelling. The overall evaluation of the HCCT-2010 measurement period with respect to meteorological and connected flow conditions resulted in the identification of 14 FCEs useful for further studies (see http://www.atmos-chem-phys.net/special_issue287.html).

In conclusion, the present study used an unprecedentedly comprehensive variety of tools, including tracer experiments, statistical measures, non-dimensional flow parameters and regional modelling, to provide a comprehensive analysis of connected flow conditions crucial for a Lagrangian-type hill cap cloud experiment. Results obtained using the statistical approach and those obtained using the experimental and modelling approach exhibited a high

degree of consistency. This is a significant result suggesting that statistical tools such as cross-correlation and COD analysis can be applied in future Lagrangian-type studies with greater confidence than before. Overall, the results of the present paper demonstrate that, under appropriate meteorological conditions, a Lagrangian-type approach is valid for hill cap cloud experiments. Finally, the methods and tools developed and applied in the present study can be used for the identification of suitable meteorological and connected airflow conditions during future Lagrangian-type hill cap cloud experiments.

Acknowledgements

This work was supported by the German Research Foundation (DFG, He 3086/15-1, DFG grant Me 3534/1-2).

References

Baines, P. G.: Topographic Effects in Stratified Flows, Cambridge University Press, Cambridge, 1995.

Baldauf, M., Seifert, A., Forstner, J., Majewski, D., Raschendorfer, M., Reinhardt, T.: Operational convective-scale numerical weather prediction with the COSMO model: Description and sensitivities. Mon. Weather Rev. 139 (12), 3887–3905, 2011.

Boucher, O., Randall, D., Artaxo, P., Bretherton, C., Feingold, G., Forster, P., Kerminen, V.-M., Kondo, Y., Liao, H., Lohmann, U., Rasch, P., Satheesh, S. K., Sherwood, S., Stevens, B., and Zhang, X. Y.: Clouds and Aerosols. In: Climate Change 2013: The Physical Science Basis. Contribution of Working Group I to the Fifth Assessment Report of the Intergovernmental Panel on Climate Change [Stocker, T. F., Qin, D., Plattner, G.-K., Tignor, M., Allen, S. K., Boschung, J., Nauels, A., Xia, Y., Bex, V., and Midgley, P. M. (eds.)]. Cambridge University Press, Cambridge, United Kingdom and New York, NY, USA, 571–657, 2013.

Bower, B. K. N., Choularton, T. W., Gallagher, M. W., Beswick, K. M., Flynn, M. J., Allen, A. G., Davison, B. M., James, J. D., Robertson, L., Harrison, R. M., Hewitt, C. N., Cape, J. N., McFadyen, G. G., Milford, C., Sutton, M. A., Martinsson, B. G., Frank, G., Swietlicki, E., Zhou, J., Berg, O. H., Mentes, B., Papaspiropoulos, G., Hansson, H. C., Leck, C., Kulmala, M., Aalto, P., Vakeva, M., Berner, A., Bizjak, M., Fuzzi, S., Laj, P., Facchini, M. C., Orsi, G., Ricci, L., Nielsen, M., Allan, B. J., Coe, H., McFiggans, G., Plane, J. M. C., Collett, J. L., Moore, K. F., and Sherman, D. E.: ACE-2 HILLCLOUD. An overview of the ACE-2 ground-based cloud experiment, Tellus B, 52, 750–778, 2000.

Bower, K. N., Choularton, T. W., Gallagher, M. W., Colvile, R. N., Beswick, K. M., Inglis, D. W. F., Bradbury, C., Martinsson, B. G., Swietlicki, E., Berg, O. H., Cederfelt, S. I., Frank, G., Zhou, J., Cape, J. N., Sutton, M. A., McFadyen, G. G., Milford, C., Birmili, W., Yuskiewicz, B. A., Wiedensohler, A., Stratmann, F., Wendisch, M., Berner, A., Ctyroky, P., Galambos, Z., Mesfin, S. H., Dusek, U., Dore, C. J., Lee, D. S., Pepler, S. A., Bizjak, M., and Divjak, B.: The Great Dun Fell Experiment 1995: an overview, Atmos Res, 50, 151–184, 1999.

Bruintjes, R. T., Clark, T. L., and Hall, W. D.: The Dispersion of Tracer Plumes in Mountainous Regions in Central Arizona - Comparisons between Observations and Modeling Results, J Appl Meteorol, 34, 971–988, 1995.

Choularton, T. W., Colvile, R. N., Bower, K. N., Gallagher, M. W., Wells, M., Beswick, K. M., Arends, B. G., Mols, J. J., Kos, G. P. A., Fuzzi, S., Lind, J. A., Orsi, G., Facchini, M. C., Laj, P., Gieray, R., Wieser, P., Engelhardt, T., Berner, A., Kruisz, C., Moller, D., Acker, K., Wieprecht, W., Luttke, J., Levsen, K., Bizjak, M., Hansson, H. C., Cederfelt, S. I., Frank, G., Mentes, B., Martinsson, B., Orsini, D., Svenningsson, B., Swietlicki, E., Wiedensohler, A., Noone, K. J., Pahl, S., Winkler, P., Seyffer, E., Helas, G., Jaeschke, W., Georgii, H. W., Wobrock, W., Preiss, M., Maser, R., Schell, D., Dollard, G., Jones, B., Davies, T., Sedlak, D. L., David, M. M., Wendisch, M., Cape, J. N., Hargreaves, K. J., Sutton, M. A., StoretonWest, R. L., Fowler, D., Hallberg, A., Harrison, R. M., and Peak, J. D.: The Great Dun Fell Cloud Experiment 1993: An overview, Atmospheric Environment, 31, 2393–2405, 1997.

Colle, B. A.: Sensitivity of orographic precipitation to changing ambient conditions and terrain geometries: An idealized modeling perspective, Journal of Atmospheric Sciences, 61, 588–606, 2004.

Colvile, R. N., Bower, K. N., Choularton, T. W., Gallagher, M. W., Wobrock, W., Hargreaves, K. J., Storeton-West, R. L., Cape, J. N., Jones, B., Wiedensohler, A., Hansson, H.-C., Wendisch, M., Acker, K., Wieprecht, W., Pahl, S., Winkler, P., Berner, A., and Kruisz, C.: Meteorology of the Great Dun Fell Cloud Experiment 1993, Atmospheric Environment, 31, 2407–2420, 1997.

Draxler, R., and Rolph, G.: HYSPLIT (HYbrid Single-Particle Lagrangian Integrated Trajectory) Model access via NOAA ARL READY, NOAA Air Resources Laboratory, Silver Spring, MD, 2003.

Harris, E., Sinha, B., van Pinxteren, D., Schneider, J., Poulain, L., Collett, J., D'Anna, B., Fahlbusch, B., Foley, S., Fomba, K. W., George, C., Gnauk, T., Henning, S., Lee, T., Mertes, S., Roth, A., Stratmann, F., Borrmann, S., Hoppe, P., and Herrmann, H.: In-cloud sulfate addition to single particles resolved with sulfur isotope analysis during HCCT-2010, Atmos Chem Phys, 14, 4219–4235, 2014.

Harris, E., Sinha, B., van Pinxteren, D., Tilgner, A., Fomba, K. W., Schneider, J., Roth, A., Gnauk, T., Fahlbusch, B., Mertes, S., Lee, T., Collett, J., Foley, S., Borrmann, S., Hoppe, P., and Herrmann, H.: Enhanced Role of Transition Metal Ion Catalysis During In-Cloud Oxidation of SO_2, Science, 10, 727–730, 2013.

Heinold, B., Tilgner, A., Jaeschke, W., Haunold, W., Knoth, O., Wolke, R., and Herrmann, H.: Meteorological characterisation of the FEBUKO hill cap cloud experiments, Part II: Tracer experiments and flow characterisation with nested non-hydrostatic atmospheric models, Atmospheric Environment, 39, 4195–4207, 2005.

Heintzenberg, J., and Charlson, R. J.: Clouds in the perturbed climate system : Their relationship to energy balance, atmospheric dynamics, and precipitation, MIT Press, Cambridge, MA, USA, 57 pp., 2009.

Herrmann, H., Wolke, R., Müller, K., Brüggemann, E., Gnauk, T., Barzaghi, P., Mertes, S., Lehmann, K., Massling, A., Birmili, W., Wiedensohler, A., Wieprecht, W., Acker, K., Jaeschke, W., Kramberger, H., Svrcina, B., Bächmann, K., Collett, J. L. J., Galgon, D., Schwirn, K., Nowak, A., Pinxteren, D. v., Plewka, A., Chemnitzer, R., Rüd, C., Hofmann, D., Tilgner, A., Diehl, K., Heinold, B., Hinneburg, D., Knoth, O., Sehili, A. M., Simmel, M., Wurzler, S., Majdik, Z., Mauersberger, G., and Müller, F.: FEBUKO and MODMEP: Field measurements and modelling of aerosol and cloud multiphase processes, Atmospheric Environment, 39, 4169–4183, 2005.

Jarvis, A., Reuter, H. I., Nelson, A., Guevara, E.: Hole-filled SRTM for the globe Version 4, available from the CGIAR-CSI SRTM 90m Database (http://srtm.csi.cgiar.org, last access: 18 June 2014), 2008.

Jiang, Q. F.: Moist dynamics and orographic precipitation, Tellus A, 55, 301–316, 2003.

Krudysz, M. A., Froines, J. R., Fine, P. M., and Sioutas, C.: Intra-community spatial variation of size-fractionated PM mass, OC, EC, and trace elements in the Long Beach, CA area, Atmospheric Environment, 42, 5374–5389, 2008.

Möller, D.: Chemistry of the Climate System, Walter de Gruyter, Berlin, 722 pp., 2010.

Ott, D. K., Kumar, N., and Peters, T. M.: Passive sampling to capture spatial variability in PM10-2.5, Atmospheric Environment, 42, 746–756, 2008.

Pierrehumbert, R. T., and Wyman, B.: Upstream Effects of Mesoscale Mountains. Journal of Atmospheric Sciences, 42 (10), 977–1003, 1985.

Pinto, J. P., Lefohn, A. S., and Shadwick, D. S.: Spatial variability of PM2.5 in urban areas in the United States, J Air Waste Manage, 54, 440–449, 2004.

Pruppacher, H. R., and Jaenicke, R.: The Processing of Water-Vapor and Aerosols by Atmospheric Clouds, a Global Estimate, Atmos Res, 38, 283–295, 1995.

Ravishankara, A. R.: Heterogeneous and multiphase chemistry in the troposphere, Science, 276, 1058–1065, 1997.

Rolph, G. D.: Real-time Environmental Applications and Display sYstem (READY) Website (http://ready.arl.noaa.gov). NOAA Air Resources Laboratory, Silver Spring, MD. 2013.

Sander, R.: Compilation of Henry's Law Constants for Inorganic and Organic Species of Potential Importance in Environmental Chemistry (Version 3), http://www.henrys-law.org (last access: 15 July 2013), 1999.

Schättler, U., Doms, G., Schraff, C.: A description of the nonhydrostatic regional COSMO-model part VII: User's GuideRep., Deutscher Wetterdienst, Offenbach. 2012.

Spiegel, J. K., Aemisegger, F., Scholl, M., Wienhold, F. G., Collett Jr., J. L., Lee, T., van Pinxteren, D., Mertes, S., Tilgner, A., Herrmann, H., Werner, R. A., Buchmann, N., and Eugster, W.: Temporal evolution of stable water isotopologues in cloud droplets in a hill cap cloud in central Europe (HCCT-2010), Atmos Chem Phys, 12, 11679–11694, 2012.

Strunk, M., Engel, A., Schmidt, U., Volk, C. M., Wetter, T., Levin, I., and Glatzel-Mattheier, H.: CO2 and SF6 as stratospheric age tracers: consistency and the effect of mesospheric SF6-loss, Geophys Res Lett, 27, 341–344, 2000.

Tilgner, A., Heinold, B., Nowak, A., and Herrmann, H.: Meteorological characterisation of the FEBUKO hill cap cloud experiments, Part I: Synoptic characterisation of measurement periods, Atmospheric Environment, 39, 4185–4194, 2005.

USEPA: Air Quality Criteria for Particulate Matter, National Center for Environmental Assessment, Office of Research and Development, US Environmental Protection Agency, Research Triangle Park, NC 27711, Washington, DC, Report No. EPA/600/P-99/002aF and EPA/600/P-99/002bF, 2004.

van Pinxteren, D., Brüggemann, E., Gnauk, T., Müller, K., Thiel, C., and Herrmann, H.: A GIS based approach to back trajectory analysis for the source apportionment of aerosol constituents and its first application, Journal of Atmospheric Chemistry, 67, 1-28, doi:10.1007/s10874-011-9199-9, 2010.

Vosper, S. B., Mobbs, S. D., and Gardiner, B. A.: Measurements of the near-surface flow over a hill, Q J Roy Meteor Soc, 128, 2257–2280, 2002.

Wang, Y. G., Hopke, P. K., and Utell, M. J.: Urban-scale Spatial-temporal Variability of Black Carbon and Winter Residential Wood Combustion Particles, Aerosol Air Qual Res, 11, 473–481, 2011.

Wobrock, W., Schell, D., Maser, R., Jaeschke, W., Georgii, H. W., Wieprecht, W., Arends, B. G., Mols, J. J., Kos, G. P. A., Fuzzi, S., Facchini, M. C., Orsi, G., Berner, A., Solly, I., Kruisz, C., Svenningsson, I. B., Wiedensohler, A., Hansson, H. C., Ogren, J. A., Noone, K. J., Hallberg, A., Pahle, S., Schneider, T., Winkler, P., Winiwarter, W., Colcile, R., Choularton, T. W., Flossmann, A. I., and Borrman, S.: The Kleiner Feldberg cloud experiment 1990: An overview, Journal of Atmospheric Chemistry, 19, 3–35, 1994.

Wongphatarakul, V., Friedlander, S. K., and Pinto, J. P.: A comparative study of PM2.5 ambient aerosol chemical databases, Environ Sci Technol, 32, 3926–3934, 1998.

Tables

Table 1: Dates, times (CEST), and average meteorological conditions at the Mt. Schmücke summit site during SF_6 tracer experiments (TE).

		TE1	TE2	TE3	TE4
Date		20-09-2010	23-09-2010	06-10-2010	23-10-2010
SF_6 release time		11:45–11:55	12:50–13:00	13:30–13:50	10:00–10:20
Sampling time		11:45–12:45	12:50–13:45	13:30–14:30	10:00–11:00
Meteorological conditions at Mt. Schmücke					
Temperature (°C)		7.5	14.5	10.3	-1.8
Relative humidity (RH, %)		76	68	99	94
Pressure (hPa)		907	905	905	901
Wind speed (m s^{-1})		7.8	6.5	3.8	9.0
Wind direction (°)		240	218	220	223
Global radiation (W m^{-2})		251	548	194	280
Cloud present at Mt. Schmücke?		No	No	Yes	Yes
Connected flow parameters					
COD_{O3}	GL-SM	0.13	0.07	0.12	0.29
	SM-GB	0.03	0.07	0.04	0.12
	GL-GB	0.12	0.02	0.11	0.39
COD_{N49nm}	GL-SM	0.03	0.30	0.08	0.25
	SM-GB	0.08	0.06	0.05	0.11
	GL-GB	0.08	0.33	0.08	0.31
COD_{N217nm}	GL-SM	0.03	0.06	0.45	0.20
	SM-GB	0.03	0.04	0.37	0.18
	GL-GB	0.02	0.06	0.10	0.31

Table 2. Classification of a) the general weather situations and the associated predominant air masses during the HCCT-2010 field campaign and b) the offline-measurement periods (*i.e.* periods during which both offline and online sampling were conducted).

Date	General weather situation [a]	Predominant air mass [b]	Offline-measurement periods (CEST)
14 Sept.	Trough Central Europe (TrM)	Marine air from North Atlantic (mPt)	14-09-2010 11:00 – 15-09-2010 02:00
15-17 Sept.	Cyclonic West (WZ)	Greenlandic polar air (mP)	
18-23 Sept.	Bridge over Central Europe (BM)	Warmed polar air (mPt)	
24 Sept.	Transition (Ü)	Greenlandic polar air (mP)	24-09-2010 23:45 – 25-09-2010 01:45
25-28 Sept.	Trough Central Europe (TrM)	Greenlandic polar air (mP)	
29 Sept. – 03 Oct.	High over Fennoscandia, cyclonic (HFZ)	Continental tropical air (cTp)	01-10-2010 22:30 – 02-10-2010 05:30; 02-10-2010 14:30 – 02-10-2010 20:00
04-09 Oct.	Anticyclonic South (SA)	Mediterranean tropical air (mTs)	06-10-2010 12:15 – 07-10-2010 03:15
10-14 Oct.	High over Norwegian Sea and Iceland, anticyclonic (HNA)	Continental polar air (cP)	
15 Oct.	Transition (Ü)	Continental air Central Europe (cPt)	
16-21 Oct.	Trough Central Europe (TrM)	Greenlandic polar air (mP)	19-10-2010 21:30 – 20-10-2010 03:30
22-24 Oct.	Cyclonic West (WZ)	Arctic polar air (mPa)	24-10-2010 01:30 – 24-10-2010 08:45; 24-10-2010 09:15 – 24-10-2010 11:45

[a] Subjective Hess-Brezowsky classification (Hess and Brezowsky, 1952; revised by Gerstengarbe et al., 1999);

[b] European air-mass classification (after Scherhag (1948)).

Table 3. Description of cloud conditions and overview of the statistical analysis of connected flow. mean coefficient of divergence (COD) values; cloud liquid water content (LWC); and wind direction (dd), speed (ff), and precipitation (RR, total precipitation amount during the FCE) at the Mt. Schmücke summit site are presented for each FCE.

FCE (time (CEST))	**LWC**	**dd SM**	**ff SM**	**COD SM-GL O_3**	**COD GB-SM O_3**	**COD GB-GL O_3**	**COD SM-GL N49nm**	**COD GB-SM N49nm**	**COD GB-GL N49nm**	**COD SM-GL N217nm**	**COD GB-SM N217nm**	**COD GB-GL N217nm**	**RR SM**
	g m^{-3}	**deg**	**m s^{-1}**										**mm**
FCE1.1 (14.09.10 11:00 –15.09.10 01:50**)**	0.25	236	8.2	0.06	0.04	0.03	0.06	0.08	0.03	0.74	0.75	0.14	1.2
FCE1.2 (15.09.10 03:00 – 15.09.10 06:20**)**	0.20	231	9.6	0.04	0.05	0.03	0.04	0.04	0.02	0.86	0.88	0.13	0.4
FCE2.1 (15.09.10 23:00 – 16.09.10 02:00**)**	0.17	240	8.7	0.02	0.02	0.02	0.03	0.08	0.09	0.71	0.72	0.09	0.0
FCE4.1 (16.09.10 13:10 – 16.09.10 15:00**)**	0.13	243	7.4	0.06	0.03	0.04	0.09	0.10	0.17	0.57	0.51	0.14	0.8
FCE5.1 (16.09.10 21:40 – 16.09.10 23:50**)**	0.30	239	6.3	0.05	0.03	0.03	0.04	0.10	0.12	0.89	0.87	0.13	0.0
FCE7.1 (24.09.10 21:10 – 25.09.10 00:50**)**	0.20	228	6.7	0.04	0.04	0.03	0.05	0.09	0.12	0.69	0.67	0.07	0.0
FCE11.2 (01.10.10 20:50 – 02.10.10 03:10**)**	0.37	222	3.7	0.08	0.10	0.14	0.09	0.06	0.12	0.59	0.51	0.15	0.0
FCE11.3 (02.10.10 07:10 – 03.10.10 00:30**)**	0.32	220	6.3	0.12	0.09	0.06	0.13	0.08	0.14	0.76	0.69	0.17	0.5
FCE13.3 (06.10.10 06:50 – 07.10.10 01:00**)**	0.32	223	4.2	0.10	0.06	0.07	0.11	0.09	0.15	0.50	0.41	0.12	0.0
FCE22.0 (19.10.10 01:50 – 19.10.10 09:00**)**	0.29	233	5.1	0.07	0.05	0.03	0.18	0.09	0.12	0.88	0.85	0.12	0.0
FCE22.1 (19.10.10 21:10 – 20.10.10 02:30**)**	0.31	248	4.7	0.07	0.05	0.09	0.09	0.04	0.09	0.83	0.78	0.13	0.2
FCE24.0 (21.10.10 22:10 – 22.10.10 10:00**)**	0.14	241	4.9	0.09	0.03	0.08	0.15	0.09	0.07	0.78	0.76	0.06	0.0
FCE26.1 (23.10.10 23:40 – 24.10.10 07:20**)**	0.19	233	9.7	0.03	0.04	0.01	0.10	0.04	0.09	0.86	0.84	0.08	0.8
FCE26.2 (24.10.10 08:40 – 24.10.10 12:20**)**	0.15	239	9.0	0.03	0.03	0.01	0.19	0.08	0.23	0.84	0.83	0.07	0.4

Table 4. Froude numbers (Fr), Richardson numbers (Ri), and rawinsonde observational data (from the Meiningen German Weather Service station) used to calculate these parameters, during or near all identified full-cloud events (FCEs) and non-cloud events (NCEs).

Date/time (CEST)	U / dd (ms^{-1})/(deg)	dΘ/dz (K m^{-1})	dU/dz (s^{-1})	N^2 (s^{-1})	Fr	Ri	Overflow y: yes;, n: no	Stability	Ozone COD	N49nm COD
14-09, 14:00	8 / 240	0.0054	0.0107	0.0002	0.85	1.62	y (decelerated)	stable	0.02	0.05
15-09, 02:00	6 / 225	0.0024	0.014	0.0001	0.68	0.42	y	stable	0.03	0.02
15-09, 14:00	6 / 235	− 0.0033	0.0186	− 0.0001	0	− 0.32	y*	unstable	0.02	0.07
16-09, 02:00	5 / 240	0.0034	0.0159	0.0001	1.13	0.46	y (decelerated)	stable	0.02	0.09
16-09, 14:00	6 / 250	− 0.0011	0.0112	0	→ 0.00	− 0.30	y*	unstable	0.04	0.17
17-09, 02:00	6 / 270	0.0049	0.0147	0.0002	1.1	0.77	y (decelerated)	stable	0.03	0.08
19-09, 14:00	6 / 250	− 0.0031	0.0086	− 0.0001	→ 0.00	− 1.40	y*	unstable	0.04	0.07
20-09, 14:00	6 / 235	0.0028	0.0106	0.0001	0.73	0.83	y	stable	0.01	0.03
22-09, 14:00	3 / 220	− 0.0017	0.0024	-0.0001	→ 0.00	− 9.31	y*	unstable	0.03	0.16
24-09, 02:00	8 / 220	0.0147	0.0209	0.0005	1.27	1.14	y (decelerated)	stable	0.06	0.05
24-09, 14:00	— / 210	—	—	—	—	—	—	—	0.03	0.13
25-09, 02:00	4 / 270	0.0032	0.0049	0.0001	1.39	4.49	y (decelerated)	stable	0.10	0.15
27-09, 02:00	5 / 270	0.0041	0.0121	0.0001	1.12	0.97	y (decelerated)	stable	0.12	0.11
27-09, 14:00	3 / 260	0.0004	0.0075	0	0.55	0.22	y	stable	0.12	0.16
28-09, 14:00	6 / 230	0.0021	0.0022	0.0001	0.73	15.22	y	stable	0.28	0.18
01-10, 14:00	3 / 340	0.0067	0.0008	0.0002	2.2	326.54	n (stagnant area)	stable	0.07	0.29
02-10, 02:00	3 /225	0.0064	0.0063	0.0002	2.33	5.6	n (stagnant area)	stable	0.13	0.08
02-10, 14:00	6 / 220	0.0034	0.0118	0.0001	0.81	0.82	y (decelerated)	stable	0.06	0.18
03-10, 02:00	6 / 220	0.0068	0.0057	0.0002	1.31	7.19	y (decelerated)	stable	0.29	0.10
03-10, 14:00	7 / 195	0.0023	0.009	0.0001	0.58	0.97	y	stable	0.03	0.20
05-10, 14:00	6 / 240	0.0063	0.0112	0.0002	1.2	1.72	y (decelerated)	stable	0.18	0.25
06-10, 02:00	5 / 220	0.0112	0.0174	0.0004	1.75	1.26	y (stagnant flow)	stable	0.17	0.06
06-10, 14:00	5 / 225	0.0027	0.0053	0.0001	0.85	3.23	y (decelerated)	stable	0.09	0.13
07-10, 02:00	5 / 240	0.0036	0.0085	0.0001	1.16	1.68	y (decelerated)	stable	0.14	0.27
07-10, 14:00	2 / 55	0.0024	0.0029	0.0001	2.43	10.03	n (stagnant area)	stable	0.05	0.21
08-10, 14:00	4 / 60	− 0.0015	0.0019	− 0.0001	→ 0.00	− 13.79	y*	unstable	0.11	0.08
09-10, 14:00	6 / 80	0.0032	0.0151	0.0001	0.85	0.48	y (decelerated)	stable	0.13	0.14
10-10, 02:00	7 / 85	0.0151	0.0219	0.0005	1.66	1.09	y (stagnant flow)	stable	0.09	0.09
11-10, 02:00	7 / 85	0.0187	0.0182	0.0006	1.78	1.95	y (stagnant flow)	stable	0.09	0.11
11-10, 14:00	6 / 70	0.0021	0.0155	0.0001	0.73	0.3	y	stable	0.09	0.04
12-10, 02:00	4 / 45	0.0175	0.0064	0.0006	3.32	14.76	n (stagnant area)	stable	0.11	0.06
13-10, 14:00	4 / 65	0.007	0.009	0.0002	1.83	2.97	y (stagnant flow)	stable	0.31	0.15
16-10, 02:00	4 / 245	0.0037	0.0087	0.0001	1.51	1.67	y (stagnant flow)	stable	0.12	0.20
19-10, 02:00	6 / 230	0.0062	0.0118	0.0002	1.12	1.57	y (decelerated)	stable	0.05	0.10
19-10, 14:00	7 / 230	0.002	0.0121	0.0001	0.6	0.47	y	stable	0.02	0.06
20-10, 02:00	6 / 245	0.0063	0.0185	0.0002	1.16	0.64	y (decelerated)	stable	0.06	0.07
21-10, 14:00	7 / 250	− 0.0011	0.0069	0	→ 0.00	− 0.79	y*	unstable	0.03	0.11
22-10, 02:00	7 / 240	0.0101	0.0138	0.0004	1.23	1.88	y (decelerated)	stable	0.12	0.04
23-10, 14:00	8 / 225	0.0128	0.02	0.0005	1.25	1.14	y (decelerated)	stable	0.09	0.24
24-10, 02:00	13 / 225	0.0038	0.0286	0.0001	0.42	0.16	y	stable	0.01	0.08
24-10, 14:00	7 / 245	0	0.0073	0	0	0	y	neutral	0.02	0.19

Table 5: Summary of the meteorological and overflow conditions during the identified FCEs, including a conclusive assessment of their suitability for future analyses. In brackets, the ESM section is given where the utilised material for each FCE is obtainable.

FCE Date/Time (CEST) (Offline sampling)	Remarks on meteorological conditions and flow connectivity
FCE1.1 14-09-2010 11:00 – 15-09-2010 01:50 (14-09-2010 11:00 – 15-09-2010 2:00) [ESM section A]	Mostly good overflow conditions, with low COD_{O3} (mean $COD_{O3} < 0.06$ at all sites) and COD_{N49nm} (mean $COD_{N49nm,GL\text{-}GB} < 0.08$) values, congruent O_3 concentration profiles, CODs and cross-correlation analysis showed less sufficient flow conditions around 17:30–19:00 and particularly after midnight (correlations with the upwind site were significantly lower, which indicates that slight luv blocking effects were possible), stable SW flow conditions ($dd_{SM} = 236°$), moderate wind speed ($ff_{SM} = 8.2$ m s^{-1}), precipitation at the beginning and end (total $RR_{SM} \approx 1.2$ mm) of the FCE, longest offline sampling period (15 h), cold front at the end of the FCE, frontal cloudiness, stable thermal stratification, quite stable trajectories and air mass advection, almost suitable overflow conditions predicted by the COSMO model (slightly decelerated flow particularly between 4 p.m. and 6 p.m.) **→ Suitable FCE: adequate meteorological/connected flow conditions**
FCE1.2 15-09-2010 03:00 – 06:20 (-) [ESM section B]	Good overflow conditions, with low COD_{O3} (mean $COD_{O3} < 0.05$ at all sites) and COD_{N49nm} (mean $COD_{N49nm,GL\text{-}GB} \approx 0.02$) values, very congruent O_3 concentration profiles, reasonable cross-correlations ($r_{xcor,GB\text{-}GL} \approx 0.7$), stable SW flow conditions ($dd_{SM} = 231°$), high wind speed ($ff_{SM} = 9.6$ m s^{-1}), probably stable thermal stratification, slight precipitation at all sites ($RR_{SM} \approx 0.4$ mm), increasing LWC from 0.05 to 0.28 g m^{-3}, unsteady cloud base height, short duration (3.33 h), suitable overflow conditions predicted by the COSMO model **→ Suitable, although short-duration, FCE: adequate meteorological/connected flow conditions**
FCE2.1 15-09-2010 23:00 – 16-09-2010 02:00 (-) [ESM section C]	Good overflow conditions, with low COD_{O3} (permanently below 0.02) and COD_{N49nm} (mean $COD_{N49nm,GL\text{-}GB} \approx 0.09$) values, very congruent O_3 concentration profiles, high cross-correlations ($0.6 < r_{xcor} < 0.8$), stable thermal stratification, slightly decelerated flow possible ($Fr = 1.13$), moderate to high wind speed (ff_{SM} increasing from ~7 m s^{-1} to 10.5 m s^{-1}), increasing cloud base height at the end of the FCE (> 300 m), stable SW wind conditions ($dd_{SM} \approx 240°$), relatively low LWC (mean 0.17 g m^{-3}), short duration (3 h), no precipitation, clouds probably not purely orographically induced, suitable overflow conditions predicted by the COSMO model **→ Suitable FCE: adequate meteorological/connected flow conditions**
FCE4.1 16-09-2010 13:10 – 15:00 (-) [ESM section D]	Less sufficient overflow conditions, with low COD_{O3} values (mean $COD_{O3} < 0.07$ at all sites) but high COD_{N49nm} values (mean $COD_{N49nm,GL\text{-}GB} \approx 0.17$), congruent O_3 concentration profiles but low cross-correlations, especially for the downwind site (slight disconnection possible), unstable wind direction changing from SW (224°) to WSW (254°) within 2 h, moderate wind speeds ($ff_{SM} = 7.4$ m s^{-1}), changing cloud base height (partially above 350 m at the end of the FCE), labile thermal stratification (possible entrainment), low mean LWC (0.13 g m^{-3}), slight precipitation at all sites during the event ($RR_{SM} < 0.8$ mm) due to an occlusion (frontal cloudiness), short duration (2h), suitable overflow conditions predicted by the COSMO model (but westerly winds predicted) **→ Probably useful FCE: slightly limited meteorological and connected flow conditions**

FCE Date/Time (CEST) (Offline sampling)	Remarks on meteorological conditions and flow connectivity
FCE5.1 16-09-2010 21:40 – 23:50 (-) [ESM section E]	Reasonable overflow conditions, COD_{O3} (mean $COD_{O3} < 0.05$ at all sites), COD_{N49nm} (mean $COD_{N49nm,GL\text{-}GB} \approx 0.12$), lower $COD_{N49nm,GL\text{-}SM}$ (≈ 0.04), congruent O_3 concentration profiles, moderate wind speeds ($ff_{SM} = 6.3$ m s^{-1}), stable thermal stratification, stable WSW flow conditions ($dd_{SM} = 239°$), slightly decelerated flow possible ($Fr = 1.1$), quite stable cloud base height (200–250 m), stable and high LWC (mean 0.3 g m^{-3}), no precipitation, short duration (2 h 10 min), mostly good overflow conditions predicted by the COSMO model (small upwind deceleration of the flow towards the end of the FCE) **→ Suitable, although short-duration, FCE: adequate meteorological/connected flow conditions**
FCE7.1 24-09-2010 21:10 – 25-09-2010 00:50 (24-09-2010 23:45 – 25-09-2010 01:45) [ESM section F]	Good overflow conditions, with low COD_{O3} values (mean $COD_{O3} < 0.04$ at all sites) and moderate COD_{N49nm} values (mean $COD_{N49nm,GL\text{-}GB} < 0.12$), congruent O_3 concentration profiles, very high cross-correlations ($0.8 < r_{xcor} < 0.9$), stable SW winds ($dd_{SM} = 228°$), moderate wind speeds (mean $ff_{SM} = 6.7$ m s^{-1}), orographic cloudiness, relatively stable cloud base height of ~200–250 m with an increasing LWC of ~0.1–0.3 g m^{-3}, no precipitation, quite stable thermal stratification, slightly decelerated flow possible at the end of the FCE (slight luv blocking, $Fr = 1.4$ and increasing CODs), slightly changing trajectories and air mass advection, relatively short duration (3h 40 min), conditions during the offline sampling period not as adequate as at the beginning of the FCE, suitable overflow conditions predicted by the COSMO model **→ Suitable FCE: adequate meteorological/connected flow conditions**
FCE11.2 01-10-2010 20:50 – 02-10-2010 03:10 (01-10-2010 22:30 –02-10-2010 05:30) [ESM section G]	Reasonable overflow conditions, with relatively high COD_{O3} values (mean $COD_{O3,GL\text{-}GB} \approx 0.14$) and COD_{N49nm} values (mean $COD_{N49nm,GL\text{-}GB} \approx 0.12$) and lower values just for $COD_{N49nm,SM\text{-}GB}$ (≈ 0.06), which indicates a slight luv blocking at the beginning, partially dissimilar ozone concentration profiles at the upwind site, partially high cross-correlation values, stable SW flow conditions ($dd_{SM} = 222°$), weak winds ($ff_{SM} = 3.7$ m s^{-1}), overflow possible (slight blocking effects, $Fr = 2.2$), very stable stratification, frontal cloudiness (occlusion front), slightly fluctuating cloud base height (100–200 m), increasing high LWC (mean 0.37 g m^{-3}), no precipitation, slightly changing trajectory pattern, 6h 20 min duration, conditions at the end of the offline sampling period even less adequate than during the FCE (see the COD analysis data in the ESM), less sufficient wind field conditions predicted by the COSMO model (particularly at the beginning, where small blocking effects were predicted) **→ Probably useful FCE: adequate meteorological but restricted connected flow conditions**
FCE11.3 02-10-2010 07:10 – 03-10-2010 00:30 (02-10-2010 14:30 – 20:00) [ESM section H]	Satisfactory overflow conditions, partially high COD values (mean $COD_{O3,GL\text{-}GB} \approx 0.06$; mean $COD_{N49nm,GL\text{-}GB} \approx 0.14$), with higher values mostly for the upwind site, Fr (0.8; 1.3) and Ri (0.8; 7.2) numbers indicate stable stratification and the possibility of a slightly decelerated flow, higher cross-correlations during the first half of the FCE than during the second, stable SW flow conditions ($dd_{SM} = 220°$), moderate to high wind speeds (mean $ff_{SM} = 6.3$ m s^{-1}, 3.6–9.2 m s^{-1}), slight precipitation ($RR_{SM} \approx 0.5$ mm) particularly in the first half of the FCE, frontal cloudiness (associated with a warm front), variable cloud height (100–300 m), partially high LWC values (mean 0.32 g m^{-3}), stable trajectory pattern, long duration (17h 20 min), mostly good overflow conditions predicted by the COSMO model (small upwind deceleration of the flow predicted from 20:00 onward) **→ Suitable FCE: adequate meteorological/ connected flow conditions**

FCE Date/Time (CEST) (Offline sampling)	Remarks on meteorological conditions and flow connectivity
FCE13.3 06-10-2010 06:50 – 07-10-2010 01:00 (06.10-2010 12:15 – 07-10-2010 03:15) [ESM section I]	Reasonably good overflow conditions, partially high COD values (mean $COD_{O3,GL\text{-}GB} \approx 0.07$; mean $COD_{N49nm,GL\text{-}GB} \approx 0.15$), Fr (0.85; 1.2) and Ri (3.2; 1.7) numbers indicate stable stratification and the possibility of a slightly decelerated flow, upwind site O_3 concentration profiles partially dissimilar, higher cross-correlations during the first half of the FCE than during the second (overall $r_{xcor} > 0.8$), stable SW flow conditions ($dd_{SM} = 223°$) with weak wind speeds ($ff_{SM} = 4.2$ m s^{-1}), orographic cloudiness, relative stable cloud base height (100–200 m), high LWC values (mean 0.32 g m^{-3}, $LWC_{max} = 0.58$ g m^{-3}), no precipitation, unstable trajectories, long duration (15 h), inadequate flow conditions at the end of the offline sampling event (see the COD analysis in the ESM), acceptable overflow conditions predicted by the COSMO model (upwind deceleration of the flow predicted from 20:00 onward) **→ Suitable FCE: partially adequate meteorological/ connected flow conditions**
FCE22.0 19-10-2010 01:50 – 19-10-2010 09:00 (-) [ESM section J]	Mostly good overflow conditions, relatively low COD_{O3} values (mean $COD_{O3,GL\text{-}GB} < 0.03$), COD_{N49nm} (mean $COD_{N49nm,GL\text{-}GB} < 0.12$), congruent O_3 concentrations, very high cross-correlations ($r_{xcor} > 0.9$), stable thermal stratification, slightly decelerated flow possible at the start of the FCE only (Fr = 1.1), stable SW winds (mean $dd_{SM} = 233°$), moderate wind speeds (mean $ff_{SM} = 5.1$ m s^{-1}), relatively stable cloud base height (100–200 m), moderate LWC values (0.2 - 0.4 g m^{-3}), temperature below 273 K, low clouds and slight precipitation at the end of the FCE due to an occlusion, good overflow conditions predicted by the COSMO model for the second half of the FCE (small blocking of the upwind flow/downdrafts during the first half possible) **→ Partially suitable FCE: adequate meteorological and partially restricted connected flow conditions**
FCE22.1 19-10-2010 21:10 – 20-10-2010 02:30 (19-10-2010 21:30 – 20-10-2010 03:30) [ESM section K]	Acceptable overflow conditions, reasonable COD_{O3} values (mean $COD_{O3,GL\text{-}GB} = 0.09$), COD_{N49nm} (mean $COD_{N49nm,GL\text{-}GB} = 0.09$), less congruent O_3 concentrations, reasonable cross-correlations, stable thermal stratification, slightly decelerated flow possible at the end of the FCE (Fr = 1.2), WSW to W flow conditions (mean $dd_{SM} = 248°$), low/moderate wind speed (mean $ff_{SM} = 4.7$ m s^{-1}), varying cloud height (100–200 m), almost constant LWC (mean 0.31 g m^{-3}), precipitation ($RR_{SM} < 0.2$ mm), reasonably stable trajectories, long duration (5h 20 min), flow conditions still adequate at the end of the offline sampling event (see the COD analysis in the ESM) but precipitation at all sites, stable SW winds with a small blocking of the upwind flow predicted by the COSMO model **→ Suitable FCE: adequate meteorological/ connected flow conditions**
FCE24.0 21-10-2010 22:10 – 22-10-2010 10:00 (-) [ESM section L]	Partially good overflow conditions, reasonable mean COD_{O3} ($COD_{O3,GL\text{-}GB} = 0.08$) and partially high COD_{N49nm} ($COD_{N49nm,GL\text{-}SM} = 0.15$), O_3 concentrations partly incongruent at night, good cross-correlation between the summit and downwind sites ($r_{xcor,SM\text{-}GB} \approx 0.7$), r_{xcor} for the upwind site lower (< 0.3), cross-correlation implies a slight LUV blocking at the start of the FCE, stable thermal stratification, slightly decelerated flow possible (Fr = 1.2), stable WSW flow conditions (mean $dd_{SM} = 241°$), moderate wind speed (mean $ff_{SM} = 4.9$ m s^{-1}), unsteady cloud base height (170–350 m), quite low LWC values (mean 0.14 g m^{-3}), no precipitation, temperature below 0°C, orographic cloudiness, stable trajectories, long duration (11h 50 min), COSMO model shows less stable wind arrows, with distinct blocking of the upwind flow throughout the whole event **→ Partially suitable FCE: acceptable meteorological and partially restricted connected flow conditions**

FCE Date/Time (CEST) (Offline sampling)	Remarks on meteorological conditions and flow connectivity
FCE26.1 23-10-2010 23:45 – 24-10-2010 07:20 (24-10-2010 01:30 – 08:45) [ESM section M]	Good overflow conditions, with low COD_{O3} ($COD_{O3,GL\text{-}GB} = 0.01$) and COD_{N49nm} ($COD_{N49nm} < 0.1$) values, congruent O_3 concentration profiles, high overall cross-correlations ($0.7 < r_{xcor} < 0.9$), low Fr number (Fr = 0.42), stable stratification, stable SW flow conditions (mean $dd_{SM} = 233°$), high wind speed (mean $ff_{SM} = 9.7$ m s^{-1}), inconsistent trajectories, post-frontal clouds (probably not purely orographic), relatively stable LWC (mean 0.19 g m^{-3}), variable cloud base height (300–130 m), light precipitation during the FCE ($RR_{SM} < 0.8$ mm), 7.5 h duration, flow conditions still adequate at the end of the offline sampling event (see COD analysis in the ESM) but precipitation at all sites, suitable overflow conditions predicted by the COSMO model **→ Suitable FCE with adequate meteorological/ connected flow conditions**
FCE26.2 24-10-2010 8:40 – 12:20 (24-10-2010 9:15 – 11:45) [ESM section N]	Mostly good overflow conditions, low COD_{O3} ($COD_{O3,GL\text{-}GB} = 0.01$) but rather high COD_{N49nm} ($COD_{N49nm,GL\text{-}GB} = 0.23$), congruent O_3 concentration profiles, good cross-correlations ($0.65 < r_{xcor} < 0.85$), low Fr number, SW/WSW flow conditions (mean $dd_{SM} = 239°$), high wind speed (mean $ff_{SM} = 9.0$ m s^{-1}), inconsistent trajectories, post-frontal cloudiness and precipitation ($RR_{SM} < 0.4$ mm), cloud base height ~200 m, increasing above 350 m at the end of the FCE, decreasing LWC (mean 0.15 g m^{-3}), 3h 40 min duration, suitable overflow conditions predicted by the COSMO model **→ Suitable FCE, but short event, with adequate meteorological and most likely adequate connected flow conditions**

1

2

Figures

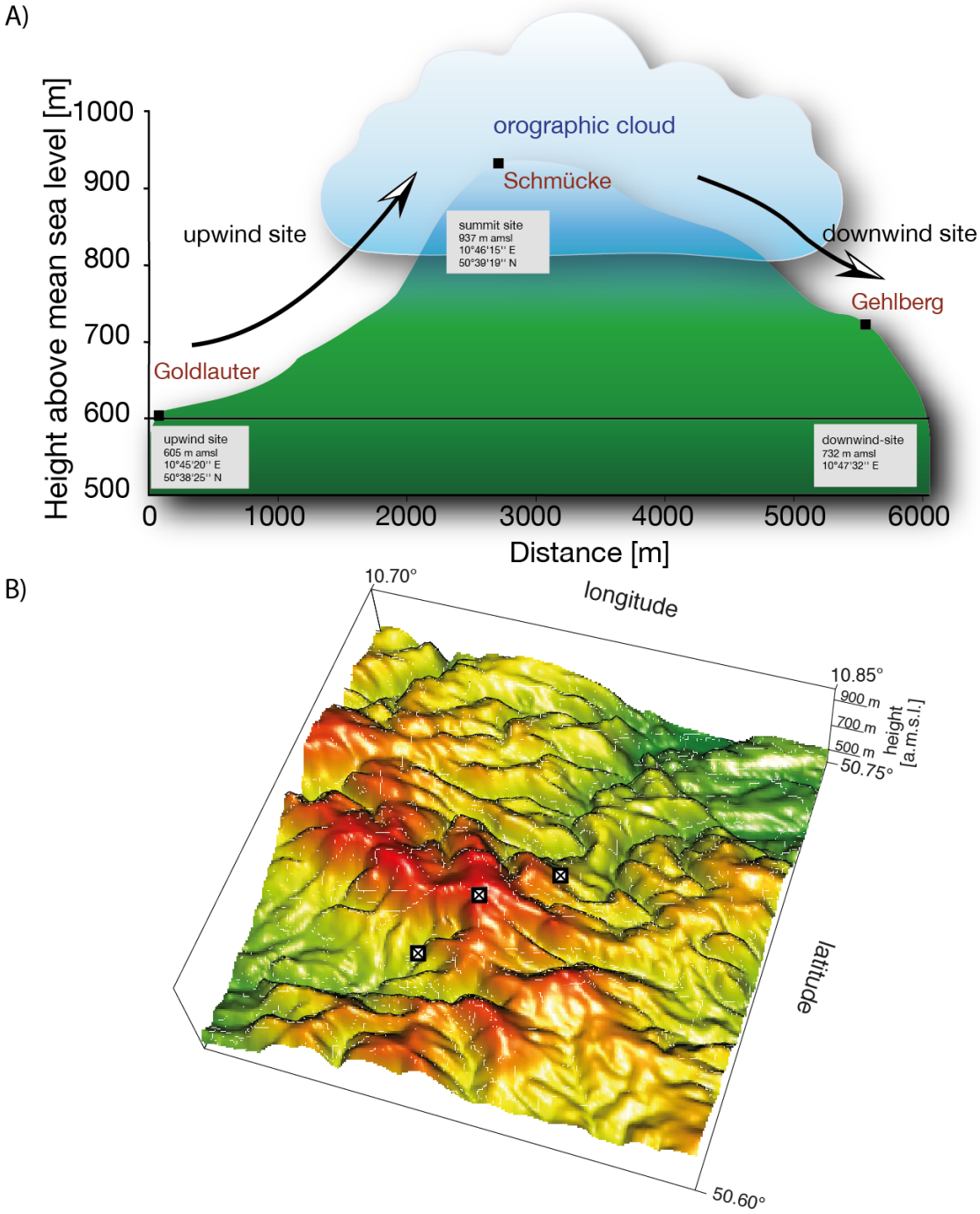

Figure 1: A) Schematic depiction of the HCCT-2010 measurement area and the three sampling sites, including the upwind site Goldlauter, the summit/in-cloud site Mt. Schmücke, and the downwind site Gehlberg. B) Depiction of the terrain of the measurement area (based on SRTM data (Shuttle Radar Topography Mission) available from the CGIAR-CSI SRTM 90m Database v4.1 (http://srtm.csi.cgiar.org/; Jarvis et al., 2014)).

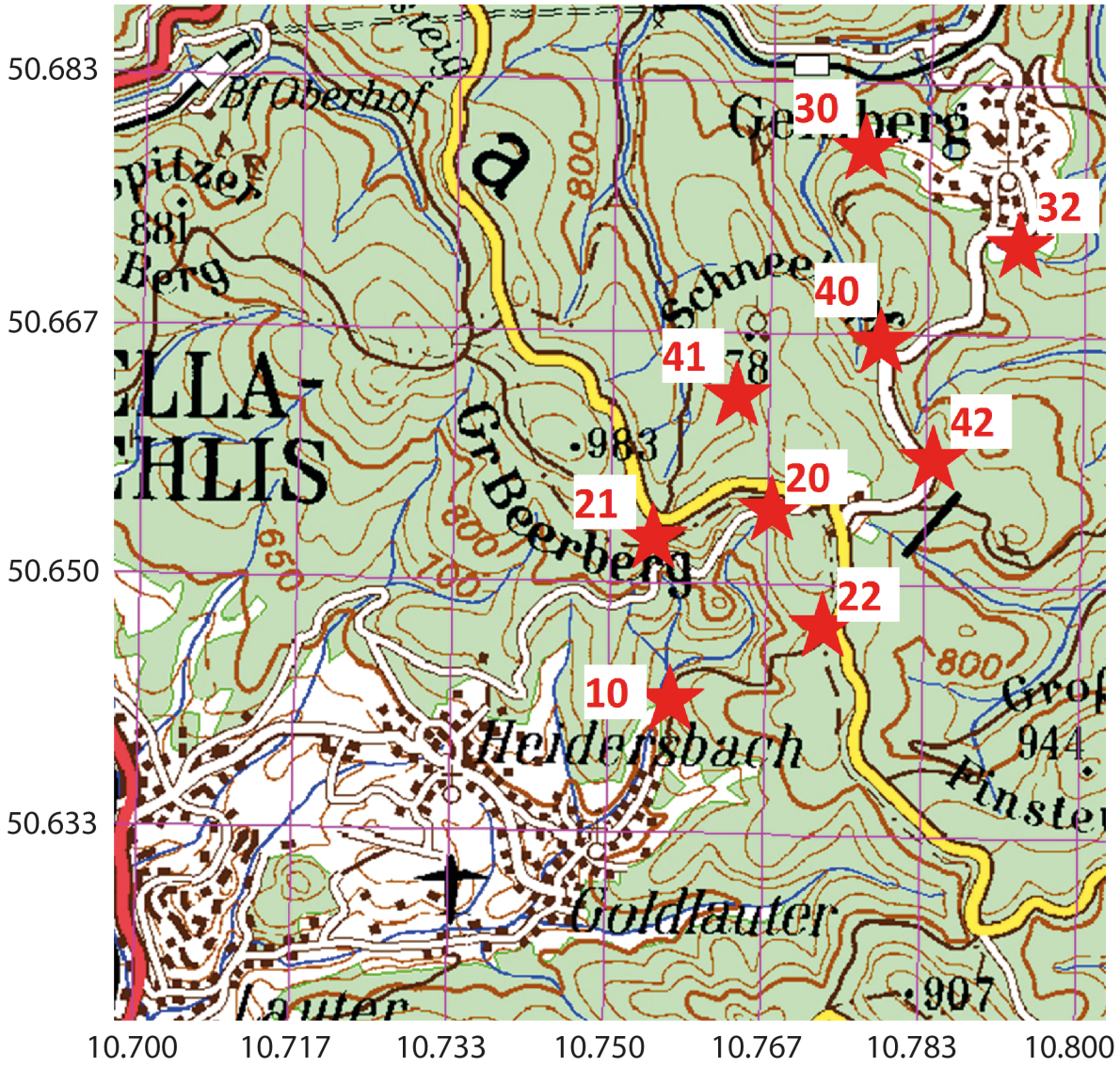

Figure 2: Locations of all tracer experiment sampling sites, including the upwind release site Goldlauter (10), the summit site Mt. Schmücke (20) and the downwind site Gehlberg (30) (Map source: Thüringer Landesvermessungsamt).

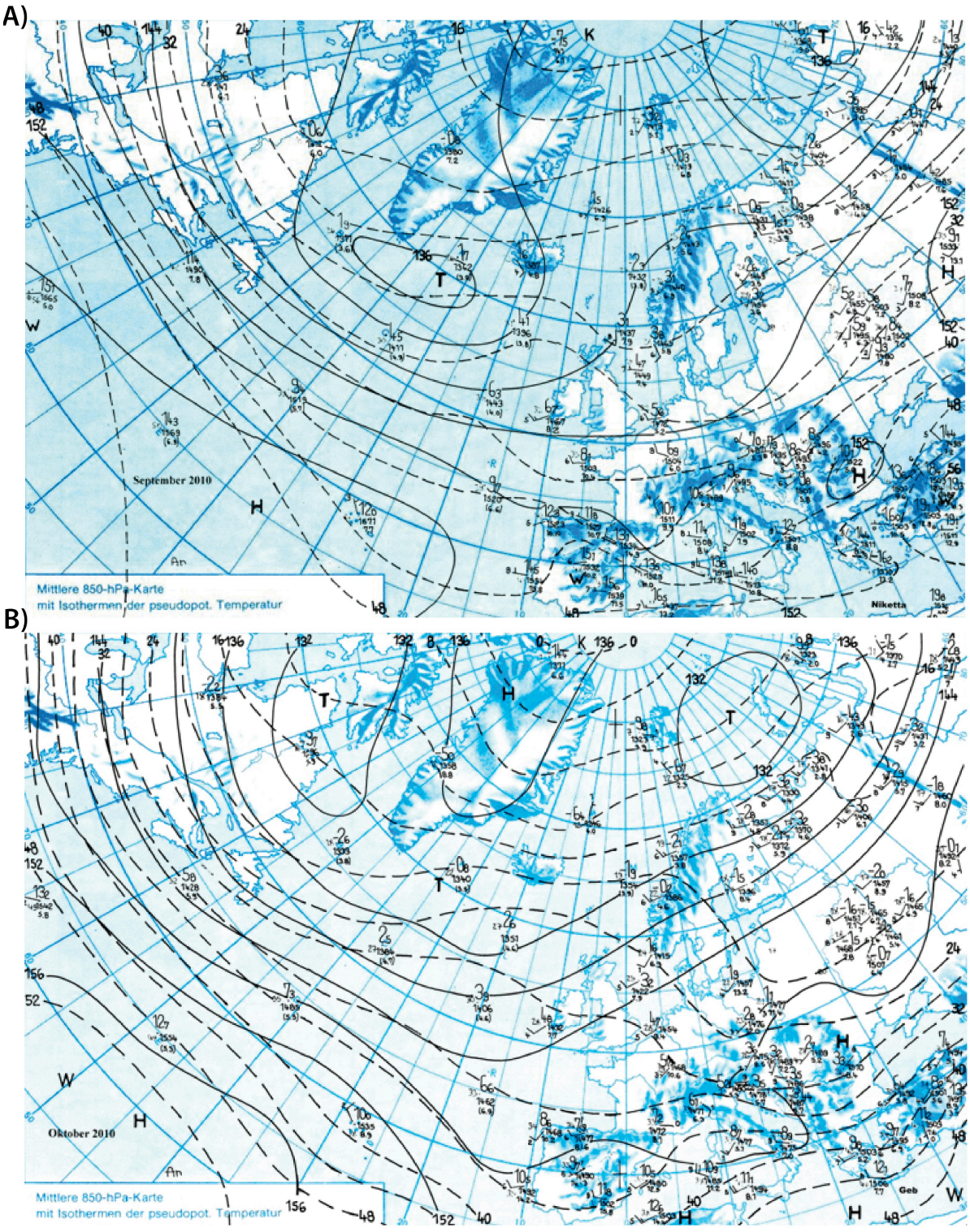

Figure 3. Averaged synoptic situation (850 hPa level) over the North Atlantic and Europe in September 2010 (A) and October 2010 (B), including isotherms of the pseudo-potential temperature (source: Berliner Wetterkarte e.V., 2010).

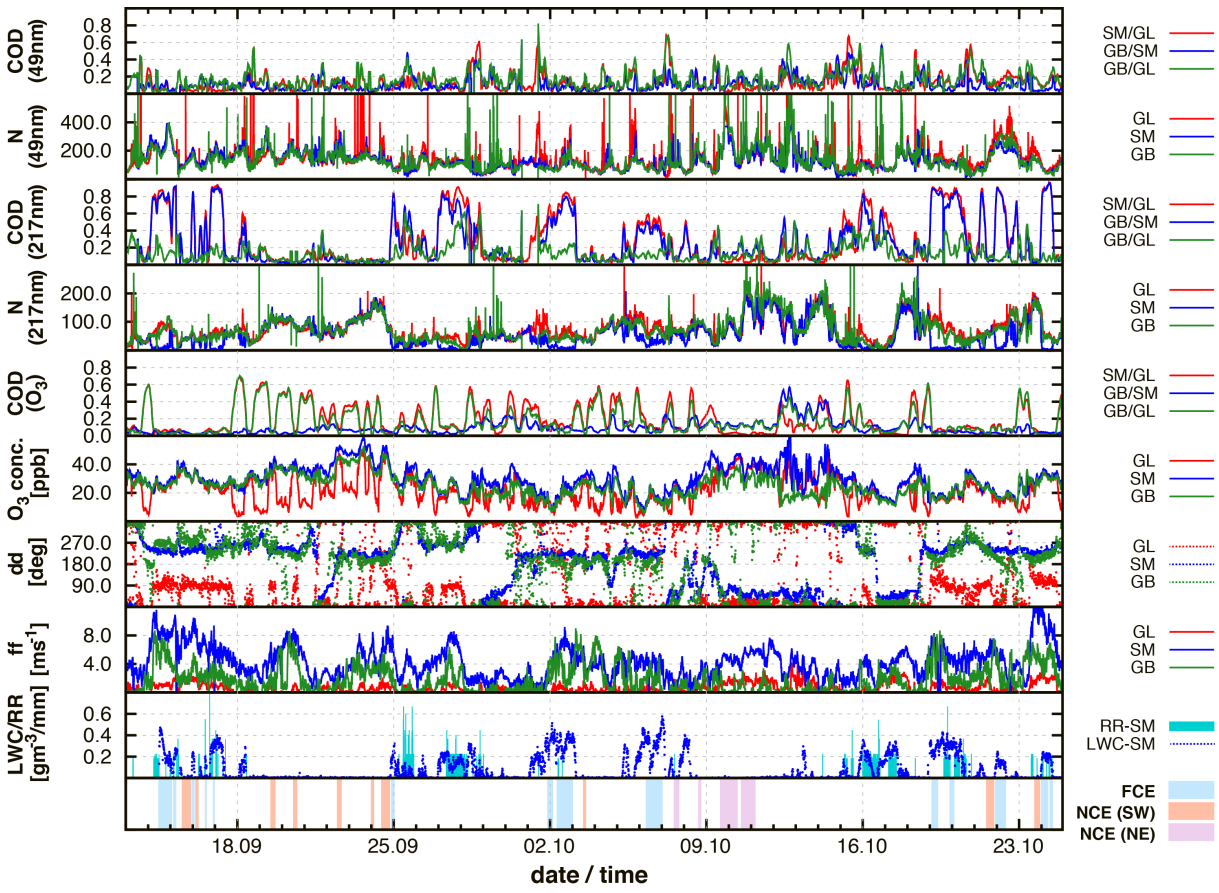

Figure 4. Depiction of the measured meteorological parameters (wind direction (dd), wind speed (ff), precipitation (RR), cloud liquid water content (LWC)), ozone and particle concentrations (size bins N_{49nm} and N_{217nm}) and the calculated COD values.

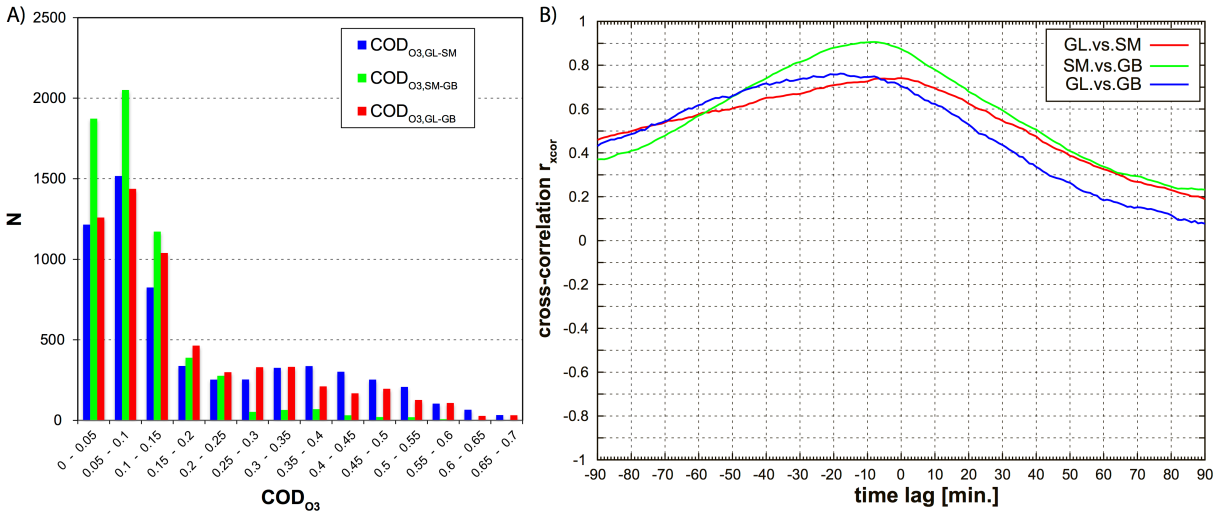

Figure 5. Histogram of the calculated COD_{O3} values throughout the whole investigation period of HCCT-2010 (A) and calculated cross-correlation (r_{xcor}) between the different sites (GL: upwind site; SM: summit site; GB: downwind site) based on measured ozone concentrations for a selected time period (B, 14-09-2010 11:00 CEST – 15-09-2010 01:00 CEST).

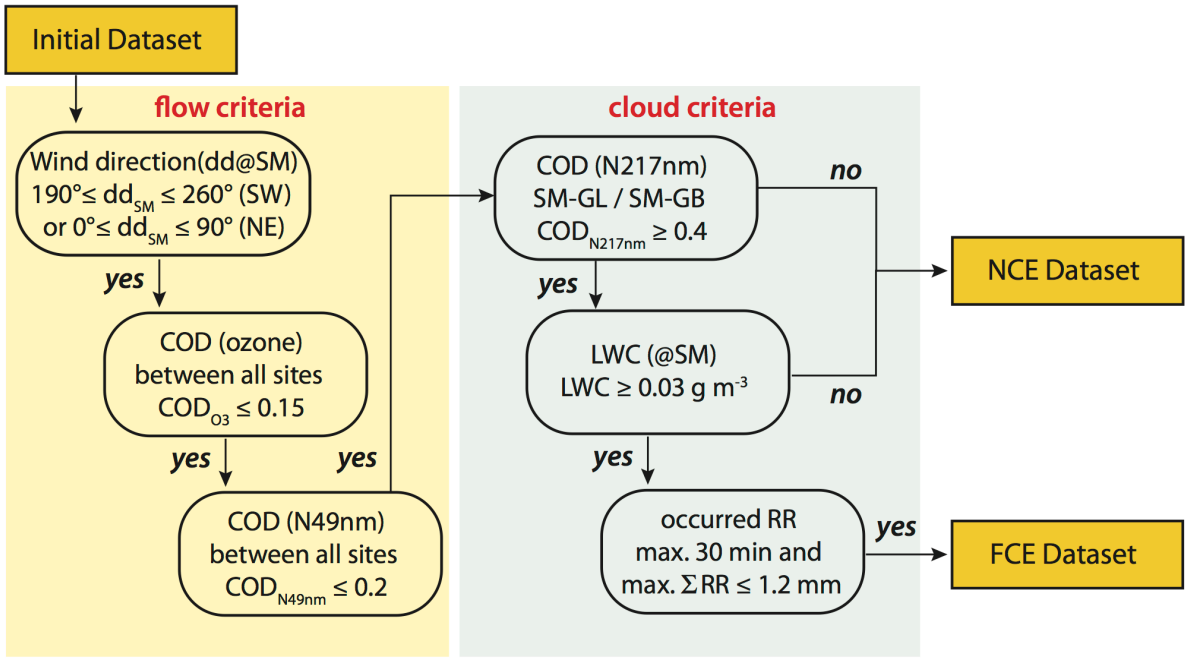

1

2 Figure 6. Schematic depiction of the FCE and NCE selection procedure.

3

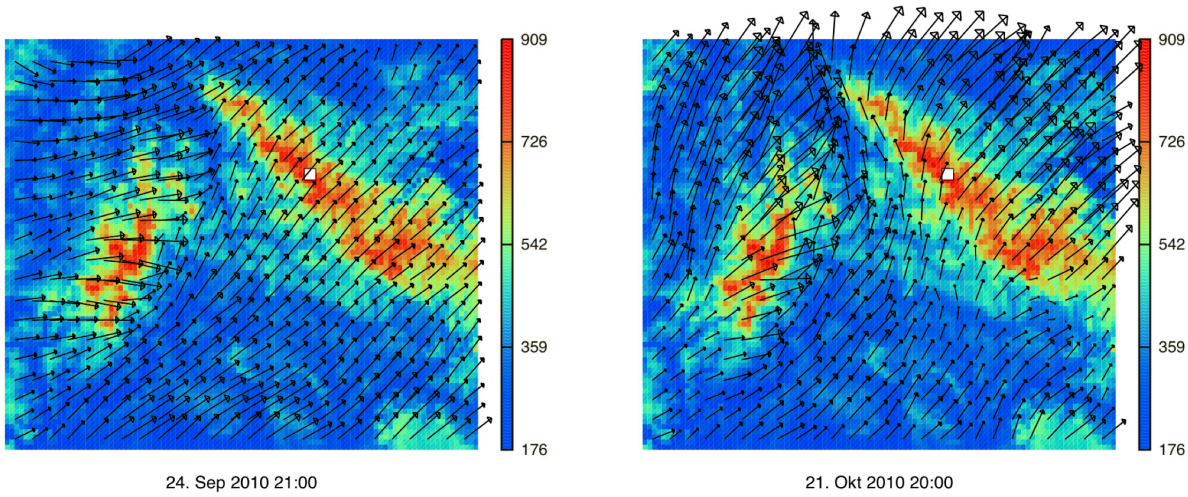

Figure 7: Depiction of the horizontal cross-section of the topography and the wind conditions (black arrows) above the ground for the COSMO model domain at 21:00 UTC on September 24, 2010 (left graphic) and at 20:00 UTC on October 21, 2010 (right graphic). The white square represents the Mt. Schmücke site.

1

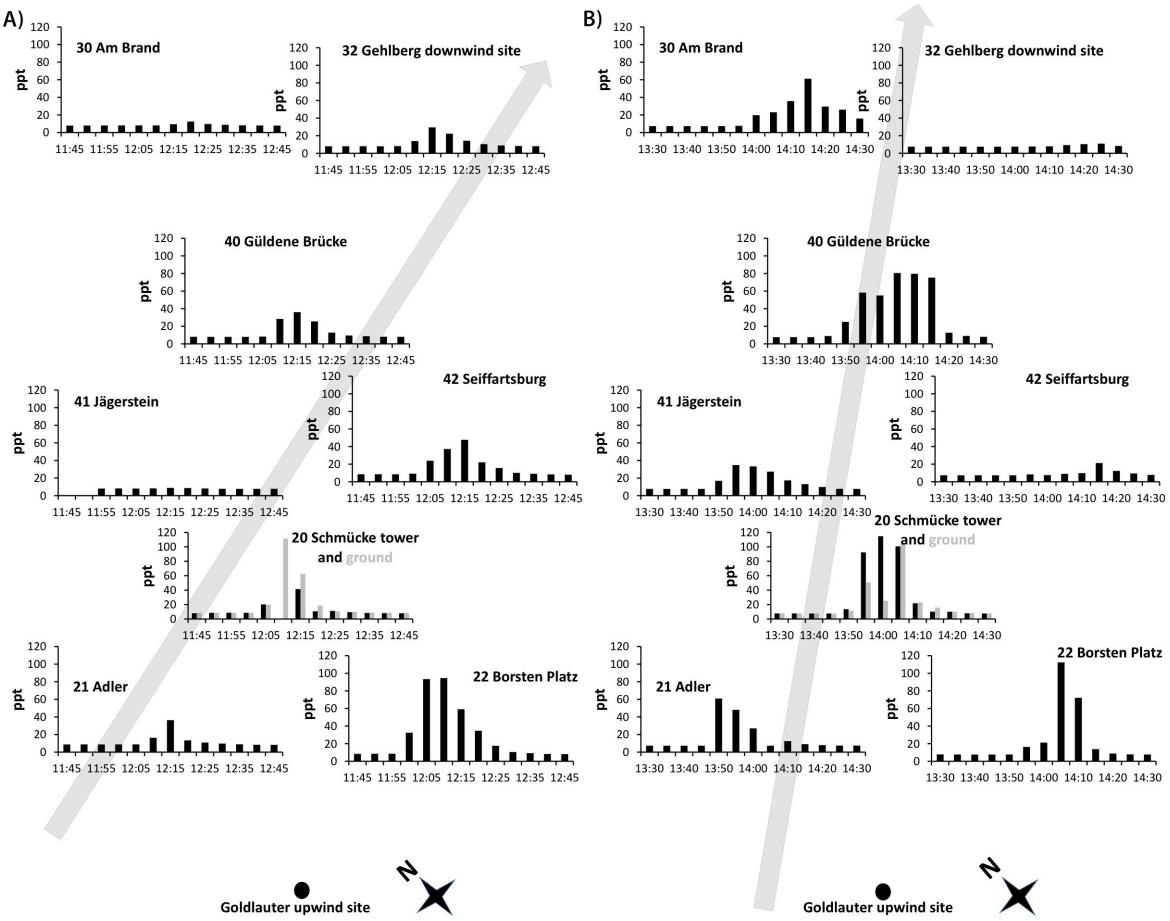

2 Figure 8: SF_6 mixing ratios at measurement sites during the (A) TE 1 and (B) TE 3 tracer
3 experiments. The positions of the bar plots indicate the approximate geographic positions of
4 the sites, and the grey arrow on each plot indicates the mean wind direction at the Mt.
5 Schmücke summit site during the experiments. SF_6 release was conducted at the upwind site
6 Goldlauter.